Impact of hydrogen and crosshead displacement rate on the martensitic transformations and mechanical properties of 304L stainless steel

Claeys, L.; De Graeve, I.; Depover, T.; Verbeken, K.

Published in:
Theoretical and Applied Fracture Mechanics

DOI:
10.1016/j.tafmec.2021.102952

Publication date:
2021

Impact of hydrogen and crosshead displacement rate on the martensitic transformations and mechanical properties of 304L stainless steel

L. Claeys[1], I. De Graeve[2], T. Depover[1], K. Verbeken[1,*]

[1]Ghent University, Department of Materials, Textiles and Chemical Engineering, Research group of Sustainable Materials Science, Technologiepark 46, 9052 Ghent, Belgium
[2]Vrije Universiteit Brussel, Department of Materials and Chemistry, Research group of Electrochemical and Surface Engineering, Pleinlaan 2, 1050 Brussels, Belgium

Lisa.Claeys@UGent.be; Iris.De.Graeve@vub.be; Tom.Depover@UGent.be

*Corresponding author: Kim.Verbeken@UGent.be

Abstract

In-situ tensile testing of electrochemically hydrogen charged 304L stainless steel at different crosshead displacement rates results in a largely different elongation at fracture compared to the corresponding test in air. At slow engineering strain rates (below 1E-2 s^{-1}), large ductility losses are observed and the alloy suffers from clear hydrogen embrittlement (HE). The HE increases with decreasing strain rate due to the increased time that is given for hydrogen to diffuse and accumulate. However, at higher engineering strain rates (above 1E-2 s^{-1}), the ductility increases with hydrogen charging. Due to intense martensitic transformations triggered by a combined temperature and hydrogen effect, the strain hardening of the alloy improves and necking is postponed. The temperature effect is restricted by reference testing in solution showing that HE still prevails. The enhanced martensitic transformations with hydrogen open opportunities for the creation of hydrogen resistant materials where the balance between HE and enhanced martensitic transformations can be optimized for the required application. Furthermore, tensile pre-straining results in an increased HE susceptibility due to the presence of stress concentrations and α'-martensite.

Please cite this article as: Claeys et al., Impact of hydrogen and crosshead displacement rate on the martensitic transformations and mechanical properties of 304L stainless steel, Theoretical and Applied Fracture Mechanics 113 (2021) 102952, https://doi.org/10.1016/j.tafmec.2021.102952

Keywords

304L stainless steel; hydrogen embrittlement; martensitic transformation; strain rate; ductility

1. Introduction

Austenitic stainless steels (ASS) are second generation advanced high strength steels. They combine a high ultimate tensile strength with a large elongation at fracture. Due to the alloying with chromium and nickel, stainless steels exhibit excellent corrosion resistance as well. AISI 304 ASS is one of the most frequently used alloys containing approximately 18% of chromium and 8% of nickel [1]. It is a major food processing material because of its high corrosion resistance and easy formability [2]. Moreover, AISI 304 ASS is used in construction and automotive industry. A big advantage is its large energy absorption capacity as needed in case of a crash [3].

Despite a relatively low yield strength, AISI 304 ASS shows a lot of strain hardening reaching high ultimate tensile strengths. The high formability while maintaining a high strength is a result of the transformation induced plasticity (TRIP) effect, i.e. the metastable austenite (γ) transforms to epsilon (ε) martensite and/or alpha prime (α') martensite under the application of strain [4, 5]. ε-martensite nucleates due to the overlap of stacking faults on every second {111} plane. Strain-induced α'-martensite is stated to nucleate at various possible locations. These include shear band intersections, isolated shear bands, shear band/grain boundary intersections and grain boundary triple junctions [6]. Kaoumi et al. [7] used in-situ TEM observation to study the deformation induced martensite transformation in AISI 304 ASS and confirmed the possibility of three different transformation routes, i.e. γ→ε, γ→ε→α' and γ→α'. Regarding the latter transformation route, these authors found that the interface migrated upon pulling of the specimen and stopped when the stage was at rest. The

transformation was thus a direct result of the applied strain. At room temperature, the transformation to α'-martensite dominates for 304L ASS [8].

The applied strain rate during tensile testing has been stated to influence the strain-induced martensitic transformations. According to Olson and Cohen [9], the martensite content decreases with decreasing strain rate as less of the previously mentioned nucleation sites are formed. Buckley et al. [10] indicated that the martensite fraction did not vary significantly for strain rates ranging from $2x10^{-6}$ to $2x10^{-3}$ s^{-1}. The inherent strain rate sensitivity of 304 ASS was thus found to be limited [11]. However, plastic deformation gives rise to adiabatic heating, which is much more pronounced at fast strain rates due to the limited time for the heat to dissipate into the surroundings. As a result, the amount of martensite and therefore also the strength and ductility, is usually reduced at high strain rates [12].

During production and in many of its applications, 304L ASS comes into contact with hydrogen. This can lead to hydrogen embrittlement (HE), i.e. a deterioration of the mechanical properties and structural integrity due to the presence of hydrogen in the microstructure [13]. Established hydrogen embrittlement mechanisms such as hydrogen-enhanced localized plasticity (HELP) [14], hydrogen-enhanced decohesion (HEDE) [15] and hydrogen-enhanced strain-induced vacancy formation (HESIV) [16] apply to face centered cubic (FCC) steels as well, despite the hydrogen diffusivity being relatively low compared to body centered cubic (BCC) steels.

Brass et al. [17] investigated the influence of the applied strain rate on the hydrogen embrittlement of cathodically precharged 304L ASS. The authors illustrated clearly that the susceptibility to hydrogen decreased with increasing strain rate. Buckley et al. [10] also found an increase in HE with decreasing strain rate for 304L ASS until a maximum was reached and the HE decreased again with decreasing strain rate. As the authors performed ex-situ tensile

tests with precharged hydrogen, a lot of hydrogen desorbed from the specimen at the low strain rates explaining the drop in HE sensitivity. Pan et al. [18] also confirmed the increasing HE sensitivity with increasing strain rate and determined a logarithmic equation for the strain rate dependency for 304L austenitic stainless steel: %HE (based on elongation) = -3.6 - 4.3*LN(strain rate).

Metastable austenitic stainless steels were found to be more prone to HE than stable austenitic stainless steels, although austenite stability was stated not to be a sufficient criterion for the HE susceptibility of austenitic steels [19]. Briant [20] reported that the most detrimental effect on the HE susceptibility of AISI 304 ASS was the formation of strain-induced α'-martensite upon deformation, especially when it was formed along grain boundaries. Han et al. [21] similarly reported that HE occurred due to strain-induced α'-martensite presence along grain boundaries in sensitized austenitic stainless steels. For cathodically hydrogen charged specimens, Wang et al. [22] showed that the HE sensitivity increased largely with increasing pre-strain level. A direct relation with the α'-martensite fraction was found. 304L ASS pre-strained at 50 and 80°C exhibited less HE due to the lower α'-martensite fraction after pre-straining [23]. The HE sensitivity at 80°C of non pre-strained 304L ASS was also lower than the HE during straining at 25°C due to suppressed formation of α'-martensite [24]. Hydrogen-induced slow crack growth did even not occur when 304 ASS was tensile tested in gaseous hydrogen atmosphere above the M_d-temperature, i.e. the temperature above which no strain-induced martensitic transformations take place [25]. Perng et al. [26] observed a high crack growth rate in 301 ASS due to the presence of α'-martensite at the crack tip. Martin et al. [27] observed that machining-induced α'-martensite at the surface of 304 ASS was detrimental for its HE resistivity. In all of the above cases, the reason for the observed increased HE sensitivity with increasing α'-martensite fraction is the large difference in hydrogen solubility and

diffusivity compared to the parent austenite phase [28]. Buckley et al. [10] observed, however, that pre-straining reduced the HE sensitivity and was independent of the amount of strain-induced α'-martensite. The produced dislocation substructures were thought to be responsible for the observed decreasing trend with pre-strain level. Zhang et al. [29] stated that prior strain-induced α'-martensite has little relation with HE while dynamic α'-martensite formed during a tensile test increased the HE sensitivity since dynamic α'-martensite is supersaturated with hydrogen upon transformation. Zhou et al. [30] stated that the type of embrittlement was important. HE increased with increasing pre-strain level for internal hydrogen, while HE reached a maximum with increasing pre-stain level for external hydrogen. The latter was explained by the reduction in dislocation main free path limiting the possible hydrogen transport distance during the tensile test following pre-straining.

Hydrogen itself is also stated to influence the operative deformation mechanisms. In-situ observations with TEM showed that hydrogen reduced the elastic interactions between obstacles and perfect or partial dislocations under constant load and therefore enhanced the dislocation mobility [31]. Most literature agrees that hydrogen increases slip planarity in austenitic steels since it reduces the stacking fault energy (SFE) and has a pinning effect on edge dislocations preventing them from cross-slipping [32, 33]. The influence of hydrogen on the martensitic transformations taking place is, however, more under debate. Several authors mention a decrease in α'-martensite fraction under the presence of hydrogen during plastic straining of 304 ASS and austenitic steels in general [34, 35, 36, 37]. Others revealed that hydrogen did not influence the martensite fraction [10]. In contradiction, an increase in α'-martensite fraction when hydrogen was present in the microstructure during straining has also been reported for austenitic stainless steels [38, 39].

Consequently, the interaction between hydrogen and deformation-induced martensite in 304L ASS is still under debate. The role of pre-existing α'-martensite on HE of 304L ASS will be evaluated in the presence of high hydrogen concentrations after cathodic hydrogen charging to validate the mentioned literature observations in the present work. Moreover, an in-depth study of the influence of hydrogen on the strain-induced martensitic transformation will be performed through electron backscatter diffraction (EBSD), which has rarely been applied in the mentioned state-of-the-art literature works and can identify both ε- and α'-martensite [40, 41]. Finally, different constant crosshead displacement rates will be applied. This will allow to evaluate the influence of hydrogen diffusion on HE of 304L ASS and to analyze the influence of strain rate on martensitic transformation (adiabatic heating effect) in the presence of hydrogen.

2. Material and methods

An AISI 304L ASS plate was used with a thickness of 0.9 mm. The steel had a reduced carbon content (denoted by L). The composition of the steel as provided by the manufacturer can be found in Table 1. Two different material conditions were studied in the present work. The first condition was the as-received 304L ASS. For the second condition, the as-received steel was pre-strained to an elongation of 30% in air in a tensile bench at a constant engineering strain rate of 1E-3 s^{-1}. Plates (140x40x0.9 mm^3) were used for this purpose. The elongation was determined based on the crosshead displacement and hence does not represent the true plastic strain.

Table 1: Chemical composition of AISI 304L ASS

Wt%	C	Cr	Ni	Mo	Mn	Si	Other
UNS S32205	0.025	18.05	8.05	0.32	1.81	1.54	Cu 0.33, P 0.031, Co 0.151, N 0.07

Microstructural characterisation was performed with scanning electron microscopy (SEM, FEI Quanta 450 FEG) equipped with electron backscatter diffraction (EBSD). The SEM was operated with an accelerating voltage of 20 kV and a spot size of 5 nm. For EBSD, a tilt angle of 70° and a step size of 0.1 µm on a hexagonal grid were used. X-ray diffraction (XRD) was used to determine the martensite phase fractions. The XRD device was operated with a Mo source at a voltage of 40 kV and a current of 40 mA. The angle 2θ was scanned from 25° to 40° with a step size of 0.006° and 5 s holding time per step.

Hydrogen was introduced by electrochemical hydrogen charging at room temperature. A constant current density of 0.8 mA/cm² was applied, which showed to be a reliable value in previous research on duplex stainless steel since it did not provoke hydrogen-induced damage [42]. The specimens were first machined from the plate material and then acted as cathode where hydrogen evolution took place, while platinum foils at both sides of the specimens acted as the anode. The used electrolyte consisted of a 0.5M H_2SO_4 solution containing 1 g/l thiourea added as a poison for the hydrogen recombination reaction. Charging was performed for seven days. As hydrogen diffusion is very slow in austenite [28], only a small region at the surface was charged with hydrogen within the applied charging time. However, an increased surface hydrogen concentration is sufficient to cause hydrogen-assisted cracking (HAC) and Enomoto et al. [43] stated that hydrogen absorption under cathodic charging and from a gaseous environment are comparable.

The hydrogen content present in the steel after the charging procedure was measured with melt extraction (Galileo G8 operated with an impulse furnace and a thermal conductivity detector). The specimens had dimensions of 8x6x0.7 mm³. The surface was polished before the start of the charging procedure. Thermal desorption spectroscopy (TDS) was performed as well. The specimen geometry was circular with a diameter of 20 mm and a thickness of 0.3

mm. The thickness was reduced with respect to the melt and tensile specimens to enlarge the fraction of material that was charged with hydrogen given that the inhomogeneous hydrogen concentration profile determines the appearance of the desorption spectrum for low-hydrogen diffusivity materials [44]. As such, the peak that represents diffusion through the uncharged bulk of the specimen is less extended over a broad temperature range and thus more clearly distinguishable from the background signal. For TDS, an infrared furnace was used for gradual heating and a quadrupole mass spectrometer was used for simultaneous hydrogen detection.

Evaluation of the mechanical properties with or without hydrogen was done by performing tensile tests at different constant crosshead displacement rates. The tensile specimens had a gauge length of 10 mm. All specimens had equal thicknesses of 0.7 ± 0.01 mm after sample preparation resulting in a rectangular cross-section of 4x0.7 mm^2. The length direction was oriented along the rolling direction of the steel plate. Both material conditions were tested at crosshead displacement rates of 19.8, 0.6 and 0.0198 mm/min which, when taking into account the initial specimen dimensions corresponds to engineering strain rates of 3.3E-2, 1E-3 and 3.3E-5 s^{-1}, respectively. The tests without hydrogen were performed in air. For the hydrogen condition, specimens were pre-charged for seven days and subsequently tested in-situ, i.e. with continuous hydrogen charging during the test. Specimen handling in between pre-charging and the tensile test in the environmental cell took about five minutes. The amount of hydrogen that was lost during this time can be considered negligible compared to what was added by the seven days pre-charging procedure. The specimens were polished to a finish of 1 µm before precharging and additionally polished with OP-U after the tensile test for microstructural analysis. The tensile tests were performed until fracture or until a pre-defined intermediate elongation.

SEM was used to study fracture surfaces and hydrogen-assisted cracking on the side surface, which is why plane thin sample were preferred over round bars. Martensitic transformations were characterized by EBSD. TSL-OIM Data analysis V7.3 software was used to analyze the measurements. Points with a confidence index (CI) below 0.1 were excluded from the measurement, which was defined based on the CI study by Field [45]. Based on the created partitions, the martensite fractions were subsequently calculated.

3. Results and discussion

3.1 Material characterisation

A representative EBSD measurement of the as-received microstructure is shown in Figure 1 (a) and (b). The observed plane was the transverse direction (TD) – rolling direction (RD) plane. The as-received 304L ASS was fully austenitic apart from some residual delta ferrite (< 1%). The grains were equiaxed with an average grain size of 3.33 ± 1.77 µm. Several annealing twins were present. Figure 1 (c) and (d) show a representative EBSD measurement of the pre-strained 304L ASS. The tensile straining direction was parallel to the rolling direction. Deformation-induced α'-martensite was clearly formed, while no ε-martensite was detected. Deformation of 304L ASS at room temperature predominantly results in the direct γ→α' transformation in addition to dislocation-related processes [8]. The α'-martensite islands were evenly dispersed through the material. Based on the area fraction, an average martensite fraction of 5.6 % was determined with EBSD.

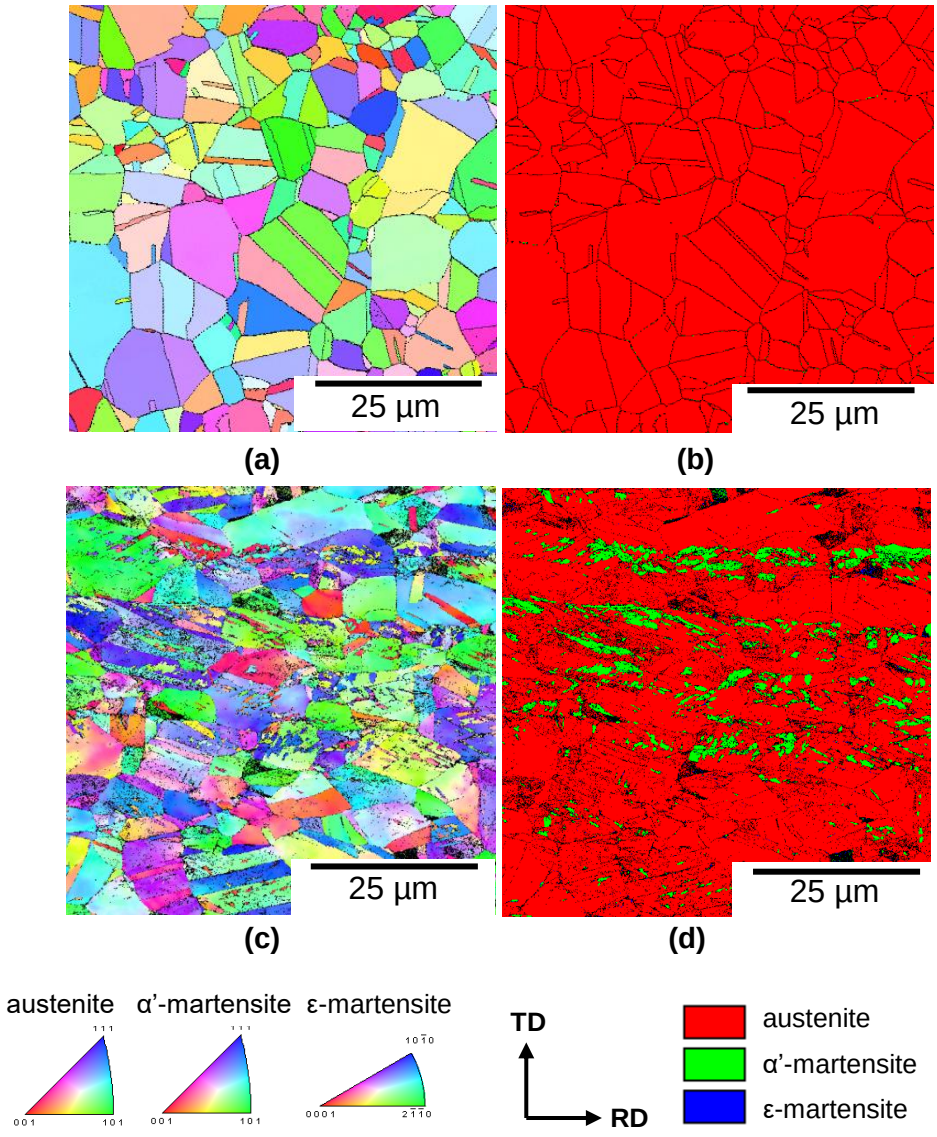

Figure 1: EBSD characterisation (ND IPF map and phase map) of as-received AISI 304L ASS in (a) and (b) and pre-strained AISI 304L ASS in (c) and (d)

XRD measurements were additionally performed to verify the martensite volume fraction in the pre-strained material. Figure 2 shows the XRD results for the as-received and pre-strained 304L ASS. The measurements showed the appearance of small peaks that could be linked to a BCC phase in the pre-strained material which were completely absent in the as-received 304L ASS. Moreover, a slight peak shift of the FCC peaks towards lower angles was observed for the pre-strained 304L ASS. The latter can be explained by the residual stresses that appeared in the austenite matrix after pre-straining due to the volume expansion of α'-martensite

compared to austenite (1.5% to 3.5% according to calculations in [46]).The formula of Cullity was used to determine the phase fraction of martensite in the pre-strained AISI 304L ASS. A martensite fraction of 4.8 vol% was found, which is in close agreement with the value found by EBSD.

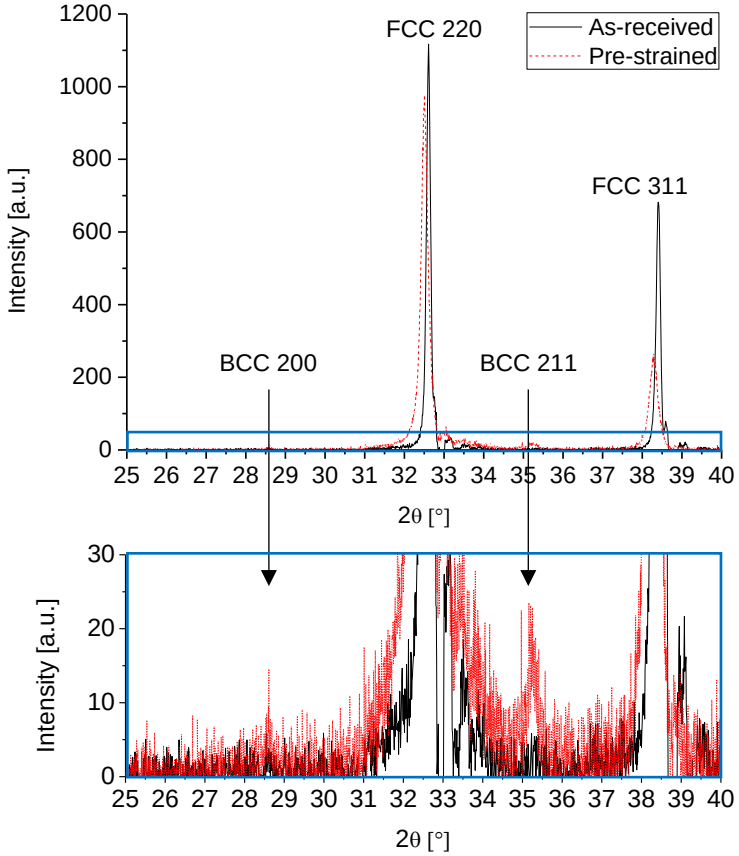

Figure 2: XRD measurements on as-received and pre-strained 304L ASS

3.2 Hydrogen/microstructure interaction

The effect of the hydrogen charging procedure on the microstructure was checked since many authors mentioned phase transformations taking place during electrochemical hydrogen charging [47, 48, 49]. In the present work, many slip bands were observed on the surface of seven days hydrogen charged as-received 304L ASS, as can be seen in Figure 3. The slip bands occurred in straight, parallel lines and are a result of plastic deformation due to the combination of hydrogen (lowers the shear modulus [50] and poses stress on the lattice) and internal stress [42]. In most cases, more than one of the {111}<110> slip systems was activated

since lines were observed in different directions within one grain. No martensitic transformations were observed as checked with EBSD for a larger scanned area (see Figure 3 (b)). The pre-existing martensite fraction in the pre-strained 304L ASS was also not changed after seven days of electrochemical hydrogen charging. More in depth hydrogen characterisation techniques were subsequently used to compare the interaction with hydrogen for the as-received and pre-strained 304L ASS.

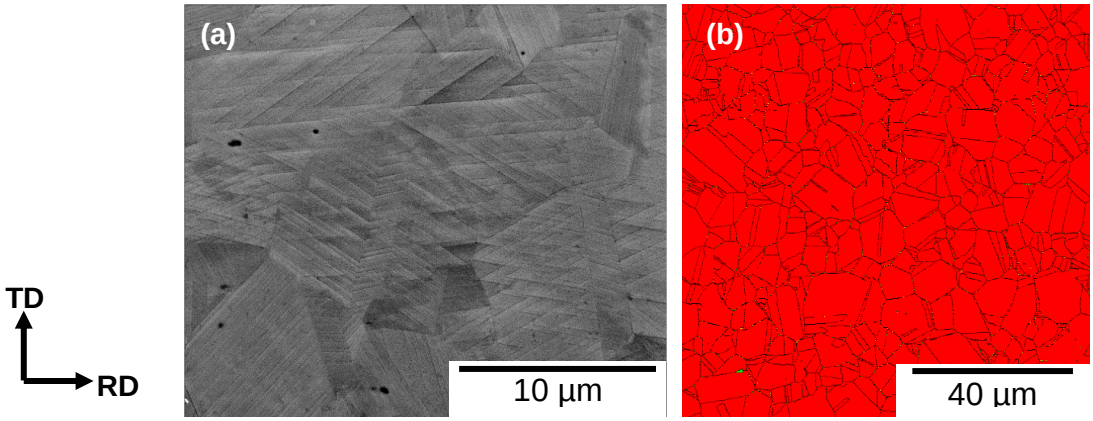

Figure 3: Surface appearance after seven days of electrochemical hydrogen charging for as-received 304L ASS (a) SE image showing slip bands and (b) phase map

Melt extraction was used to determine the total hydrogen concentration present in both materials after seven days charging at room temperature. The melt extraction tests resulted in 50.0 ± 2.2 wppm and 54.7 ± 0.5 wppm hydrogen for the as-received and pre-strained 304L ASS, respectively. The slightly higher hydrogen concentration in the pre-strained material was most likely a result of enhanced hydrogen diffusion due to the presence of about 6% α'-martensite. The difference is, however, not significant. Upon saturation, the pre-strained material is expected to have a lower hydrogen concentration due to the lower solubility of α'-martensite compared to austenite [51, 52]. Moreover, pre-straining results in residual compressive stresses. This might reduce the hydrogen solubility as well and adds to the total reduction of the hydrogen content at saturation after pre-straining.

TDS was used to evaluate the average hydrogen diffusion as diffusion is the rate-determining step for the desorption of hydrogen in FCC steels [44]. Deformation-induced features such as dislocations and vacancies are stated not to influence the hydrogen diffusivity of austenite since they are characterized by a low trapping activation energy compared to the diffusion activation energy of austenite [52, 53, 23, 43]. Figure 4 shows a plot of the tests performed at a heating rate of 600 K/h and 900 K/h for both material conditions. All spectra overall consisted of two peaks, one main peak and a high temperature shoulder. The first peak can be understood as hydrogen that diffused out of the specimen towards the nearest surface while the second peak can be understood as hydrogen that left the specimen via diffusion through the uncharged sample center and then to the sample surface driven by the lower chemical potential at these locations [54]. The peak splitting is thus a direct result of the inhomogeneous hydrogen concentration, as we demonstrated in our previous work [44]. Comparison of the spectra of both materials at the same heating rate, indicated a small shift in peak position of the two peaks. The first peak maximum shifted to a higher temperature while the second peak maximum shifted to a lower temperature. Both shifts are an indication that hydrogen diffused further into the specimen during charging in the case of pre-strained 304L ASS. For the first peak, a higher peak maximum represents a larger diffusion distance. For the second peak, hydrogen that diffused deeper into the material reduced the diffusion distance to the opposite surface. Diffusion was thus slightly faster in the pre-strained material. Mine et al. [55] similarly performed TDS measurements on severely plastically deformed 304 ASS and stated that hydrogen desorption was controlled by diffusion. Their spectra contained one peak and the peak temperature shifted to lower values with increasing pre-strain. Given that the materials were saturated with hydrogen by gaseous charging, hydrogen diffusion was thus indeed enhanced by the presence of the martensite phase.

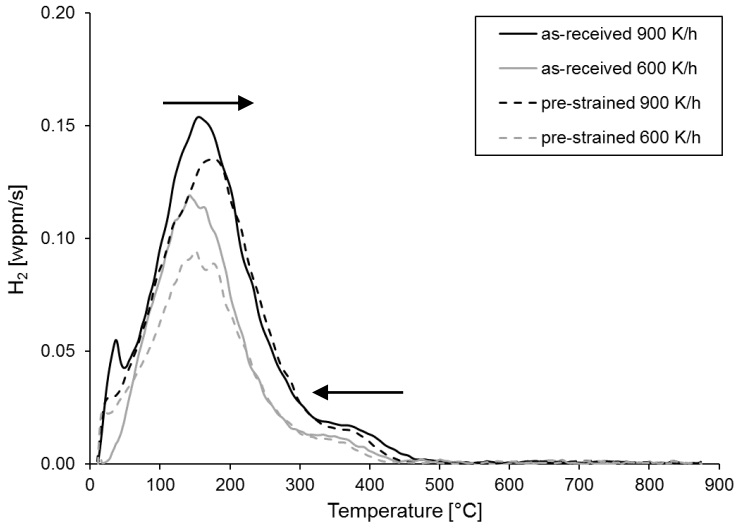

Figure 4: Thermal desorption spectroscopy data of as-received and pre-strained 304L ASS charged for 7 days at room temperature

In previous work by the authors, a model was constructed to reproduce TDS spectra based on Fick's laws for diffusion [44]. This model was used to simulate the tests that were performed in the present work as well. Both the charging and discharging processes were simulated with the appropriate boundary conditions as given in section 3.1 in [44]. The initial concentration before charging was assumed to be zero. The output of the charging simulation was used as initial condition for the discharging simulation. The boundary condition for charging was C_s at the edges while a zero boundary condition was applied for discharging. Charging occurred at a constant temperature while discharging was modelled with a constantly increasing temperature via the heating rate. The model was, however, unable to fit the mean peak and the shoulder at the same time. Intuitively, the most suitable way to obtain the effective hydrogen diffusivity of a material is by fitting the high temperature shoulder since the second peak results from diffusion through the bulk while the first peak might be prone to surface effects. A first indication of the presence of surface effects is the small increase in hydrogen flux just after the start of the measurement for some conditions (most pronounced for as-received 304L ASS at 900 K/h in Figure 4). A skin effect after electrochemical hydrogen charging was already reported in literature referring to a supersaturated hydrogen

concentration in the first few atomic layers of a material [56]. Moreover, since slip lines were clearly observed at the surface (cf. Figure 3), the effective hydrogen diffusivity might be altered compared to the bulk value. The latter is considered less of an issue for hydrogen that diffused first towards the uncharged bulk since this diffusion step will be the controlling factor in the desorption speed. The resulting least square fits for both heating rates based only on the experimental data above 200°C are presented in Figure 5. The obtained fitting parameters are given in Table 2. C_s represents the hydrogen saturation level, D_0 the pre-exponential factor of the effective hydrogen diffusivity and Q the activation energy of the effective diffusivity. At room temperature, both materials show a diffusivity in the range of 1-2x10^{-16} m²/s. Xiukui et al. [57] summarized various hydrogen permeation data of austenitic stainless steels into one expression for the temperature dependent hydrogen diffusion coefficient: D_0 = 5.76x10^{-7} m²/s, Q = 53.62 kJ/mol. The value at room temperature (295K – 1.86x10^{-16} m²/s) is similar to what was found in the present work. The slightly different temperature dependency might be related to the higher temperature range in which the authors determined their equation, i.e. 200-430°C. In the work of Perng and Altstetter [58], the D_0 and Q value were also shown to depend on the temperature range for 301 ASS. A lower temperature range resulted in higher D_0 and Q values. The hydrogen saturation level C_s is in agreement with previous work by the authors on a 50/50 austenite/ferrite duplex stainless steel which had a saturation level of about 700 wppm using the same electrolyte and charging conditions [44]. Omura et al. [59] also reported similar surface hydrogen concentration values for various stainless steels after electrochemical hydrogen charging using comparable conditions. The clear resemblance with literature data based on the fit of the high temperature shoulder indicates that the first peak was indeed influenced by a surface effect, i.e. hydrogen leaves the specimen more readily than what can be expected from its bulk hydrogen diffusivity.

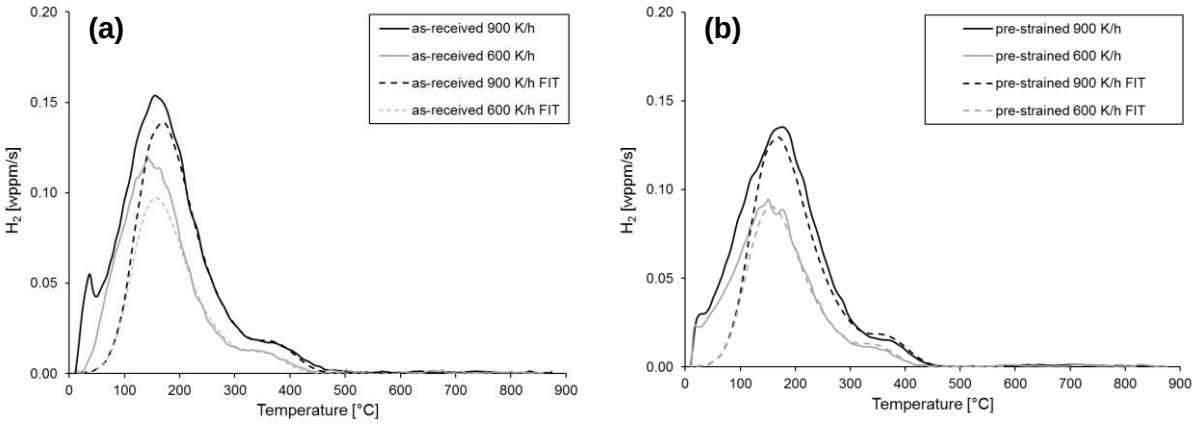

Figure 5: Diffusion fit based on Fick's laws to the experimental TDS data, the fitting procedure focused on the data above 200°C, (a) as-received 304L and (b) pre-strained 304L

Table 2: Fitting parameters of the diffusion fit to the experimental TDS data

	C_s [wppm]	D_0 [m²/s]	Q [kJ/mol]
As-received 304L	1510	2.76E-6	58.23
Pre-strained 304L	1303	2.75E-6	57.94

Figure 6 shows the calculated hydrogen concentration profile after the performed pre-charging procedure at room temperature (295K) for as-received and pre-strained 304L ASS. It is clear that only a small region (approximately 35 µm) near the surface showed an enlarged hydrogen concentration after pre-charging. It should be noted that the difference in diffusivity between both material conditions is rather small as only a small percentage of martensite was formed and the martensite islands were not interconnected.

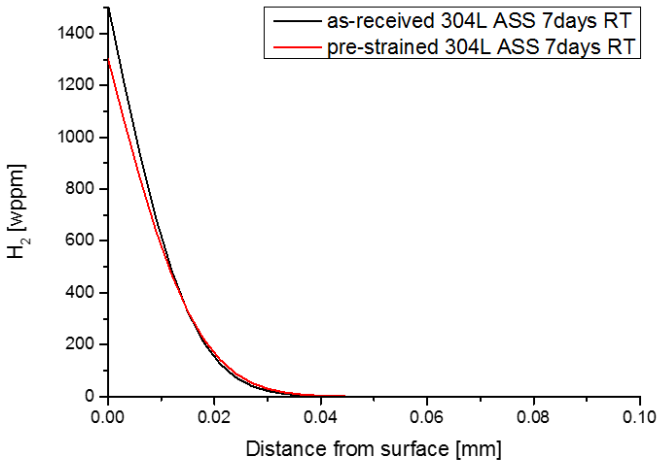

Figure 6: Hydrogen concentration profile for as-received and pre-strained 304L ASS with parameters obtained from diffusion fit to TDS data

3.3 Influence of hydrogen on the mechanical properties

Constant crosshead displacement rate tensile tests were performed to evaluate the influence of hydrogen on the mechanical properties of both materials at three different rates. The results of the tests are presented in Figure 7 (a) for as-received 304L ASS and in Figure 7 (b) for pre-strained 304L ASS. Both the reference tests performed in air and the in-situ hydrogen tests are reported. For every condition, the experiments were repeated three times to confirm the reproducibility of the tests, however, only one of the performed tests is shown. Table 3 illustrates the reproducibility of the results by showing the range of elongations at fracture at every test condition. It should be noted that the engineering strain was calculated based on the crosshead displacement. Since the strain was not measured directly due to the limitations of an environmental cell, the mentioned engineering strain rates are hence not exact but were calculated based on the constant displacement rates and the initial gauge dimensions.

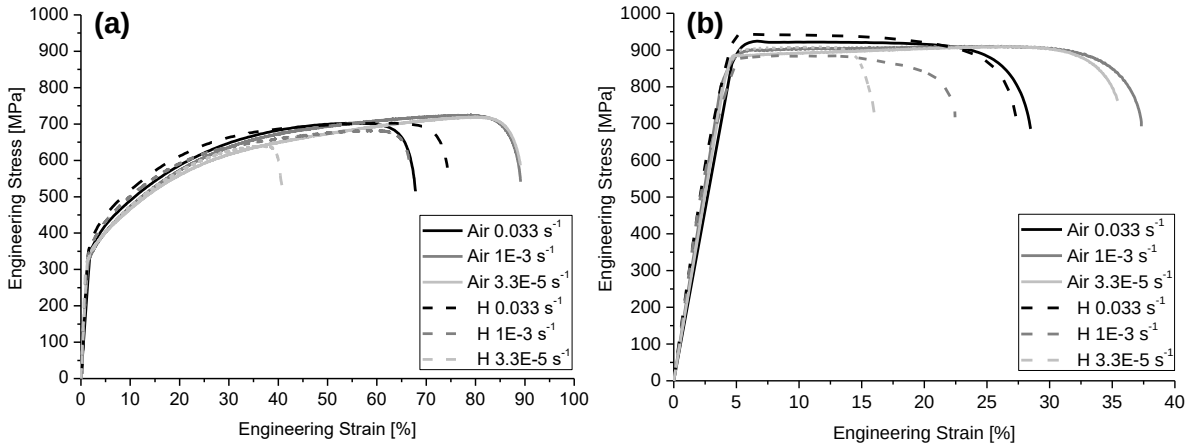

Figure 7: Engineering stress as a function of engineering strain for as-received (a) and pre-strained (b) 304L ASS

Table 3: Range of measured elongations for the different test conditions illustrating the reproducibility of the results

Engineering strain rate [s^{-1}]	As-received		Pre-strained	
	Air	Hydrogen	Air	Hydrogen
3.3E-2	65.2-68.0	74.0-75.5	25.5-27.1	26.0-27.4
1E-3	91.0-92.6	65.5-65.7	36.1-37.4	21.7-21.9
3.3E-5	85.6-88.6	36.4-40.6	34.8-35.0	13.4-15.5

The tests performed in air differed depending on the applied engineering strain rate. The faster the displacement rate, the higher the yield strength and the smaller the elongation at fracture were. Both the as-received and the pre-strained 304L ASS showed this behavior. The engineering stress-strain curves at an engineering strain rate of 1E-3 and 3.3E-5 s^{-1} were comparable for both material conditions with respect to elongation and strength at fracture. Similar strain rates were used for as-received 304L in the work of Lichtenfeld et al. [60]. The authors also reported a similar tensile behavior for strain rates in the order of 1E-3 s^{-1} to 1E-5 s^{-1}, while a reduced ultimate elongation was observed for a strain rate of 1.25E-2 s^{-1}. Talyan et al. [11] similarly reported this difference for a strain rate of 1E-2 and 1E-3 s^{-1}. The shape of their engineering stress-strain curves are also comparable to the present work. The ultimate elongation at fracture was lower (70% for 1E-3 s^{-1} compared to 90% in the present work) which is a direct result of the different strain measurement. The authors calculated the

strain based on extensometer results while the strain was calculated from the crosshead displacement in the present work. Das et al. [61] performed tensile tests on 304LN ASS and clearly indicated a constant ductility for strain rates of 1E-4 and 1E-3 s^{-1} and a continuous drop in ductility for higher strain rates. The authors also reported a continuous increase of the yield strength with increasing strain rate. Li et al. [62] performed tensile tests at different strain rates in air on 304 ASS as well. The authors also mentioned that the yield stress continuously increased with increasing strain rate. At the initial stages of deformation, martensite formation is low [62]. Dislocation slip controls the initial increase in flow stress which is enhanced at higher strain rates and thus results in a higher yield strength. At higher strain levels, martensite formation plays a dominant role in the increase in flow stress and ductility [8]. Due to adiabatic heating, less martensite is formed at high strain rates. As a result of the restiction of martensitic transformations, a lower ductility is reached [63, 6, 60, 11, 62].

Pre-straining of 304L ASS resulted in an increase in yield strength, a decrease in elongation at fracture and a decrease in work-hardening [64]. All deformation features, e.g. dislocations and martensite, that were formed during pre-straining limited the ability to accommodate additional plastic deformation during tensile testing.

Hydrogen had a large influence on the mechanical properties as illustrated by the dotted lines in Figure 7 (a) and (b). Based on the average elongation at fracture for the air and in-situ hydrogen tests, an average embrittlement index (EI) was calculated. The deviation (dev) on this value was calculated from the difference between the largest and smallest possible embrittlement index.

$$\mathrm{EI}_{\mathrm{av.}} = \frac{\mathrm{av.\,elongation\ air} - \mathrm{av.\,elongation\ H}}{\mathrm{av.\,elongation\ air}}$$

$$\mathrm{Dev} = \frac{\mathrm{EI}_{\max} - \mathrm{EI}_{\min}}{2}$$

As the elongation was calculated based on the crosshead displacement, the EI inherently contains an error and the values do not represent a true quantitative loss in ductility. This procedure is, however, frequently used for in-situ tested austenitic steels [18, 65]. Figure 8 shows the EI as a function of the engineering strain rate for the as-received and pre-strained 304L ASS.

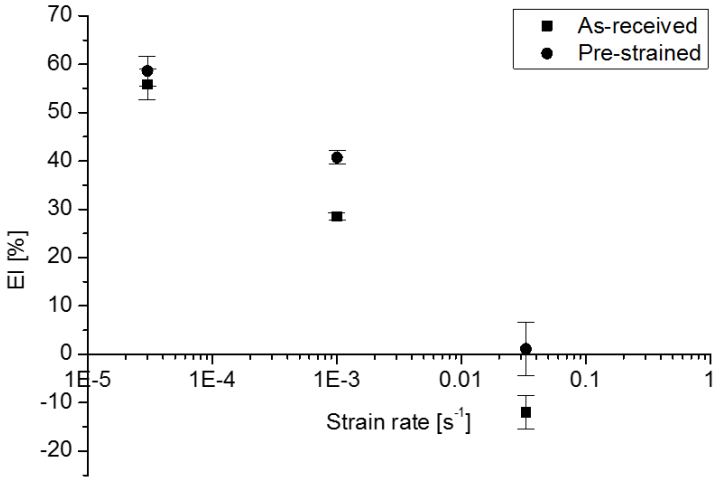

Figure 8: Embrittlement index as a function of engineering strain rate for as-received and pre-strained 304L ASS with air reference

The EI was strongly dependent on the applied strain rate for both materials. The slower the strain rate, the more sensitive both materials were to hydrogen. This is in agreement with previous observations in literature for 304 ASS [10, 17]. The values were comparable to what could be expected from the equation proposed by Pan et al. [18] at the lowest two strain rates. However, the authors performed different charging conditions compared to the present work such as precharging for 48h at 50 mA/cm² and testing in air or in-situ hydrogen charging without precharging. A one on one comparison of the results is thus not possible. An explanation for the observed strain rate dependency can be found in the time that is given for hydrogen to diffuse through the microstructure and accumulate at stress concentrations. When fast strain rates are applied, the diffusion distance is very small and the ability of hydrogen to accumulate at a crack tip or stress concentration and as such embrittle the

material is very limited. At slow strain rates, however, hydrogen diffusion is more substantial and leads to hydrogen accumulation at crack tips and subsequently hydrogen-assisted crack propagation. Hydrogen diffusion and the hydrogen concentration that can be reached as a result of diffusion at crack tips are thus determining parameters in the hydrogen embrittlement sensitivity of 304L ASS. The role of strain rate and hence hydrogen diffusion on the HE degree has been demonstrated for other materials as well and is accepted [66, 67]. The strain rate effect might be lower if the specimens were saturated with hydrogen throughout the entire thickness since concentration gradients have been eliminated then. Diffusion driven by stress gradients can, however, still occur when the material was initially saturated resulting in differences between the strain rates due to the time given for diffusion as well. The effect of strain rate was clearly illustrated for saturated specimens by Buckley et al. [10].

The pre-strained material had a higher EI for all tested strain rates which is consistent with most literature observations [27, 22, 29]. One reason might be a higher effective hydrogen diffusivity due to the formation of α'-martensite. As measured through TDS (cf. Figure 6), the difference in initial hydrogen diffusivity can, however, be regarded as insignificant in the present work. As stated in the introduction, Zhang et al. [29] also pointed out that the prior induced α'-martensite fraction has little relation with HE, especially when the fraction is low. Secondly, the pre-existing α'-martensite fraction located at the surface might provide hydrogen to the surrounding austenite matrix at a higher speed leading to crack initiation. Finite element studies have shown that it is definitely possible that the reason for HE in metastable ASS is related to the drastically increased hydrogen concentration in austenite that is located in the close neighborhood of martensite islands [68]. Other deformation-induced features (e.g. dislocations) that were formed during pre-straining might additionally have led

to a higher embrittlement of the pre-strained steel as the stress concentrations associated with e.g. dislocation pile-ups attract and accumulate hydrogen. With decreasing strain rate, the EI of the as-received and pre-strained 304L ASS approached each other. The test time became less of a limiting factor when the strain rate was very low and the formation of large stress concentrations followed by hydrogen diffusion and accumulation was not limited anymore.

One remarkable observation deserves more attention. At a strain rate of 3.3E-2 s^{-1}, the EI was negative for the as-received material, i.e. a higher elongation at fracture was observed in the hydrogen charged condition compared to the air test. As mentioned previously, at fast strain rates, adiabatic heating reduced the elongation at fracture due to restricted martensitic transformation. The surface temperature of the as-received 304L ASS reference test in air at a strain rate of 3.3E-2 s^{-1} was measured with a K-type thermocouple point welded to the gauge section. A temperature increase of 20°C was measured at the surface of the specimen during a short time interval as can be seen in Figure 9 (a). The temperature increase might be higher in the bulk. In the work of Talyan et al. [11], the temperature increased with about 20°C as well for a strain rate of 1E-2 s^{-1}. Moreover, alternative reference tensile tests were performed where the adiabatic heating effect was counteracted by a surrounding solution rather than air (in-situ cell with demineralized water) as well. The results for the as-received 304L ASS performed at 3.3E-2 s^{-1} and 1E-3 s^{-1} are given in Figure 9 (b). At an engineering strain rate of 3.3E-2 s^{-1}, the macroscopic tensile curve reached both a higher UTS and a higher elongation at fracture. Similar results for the reference test in air and in solution were, however, obtained at a strain rate of 1E-3 s^{-1}. The adiabatic heating effect is thus only important for the fastest strain rate in the present work. Other authors reported similar threshold values (order of 1E-2 s^{-1}) for the occurrence of an adiabatic heating effect as a function of strain rate for 304

ASS [60]. Talyan et al. [11] measured the temperature at a strain rate of 1E-3 s^{-1} and observed a more or less constant temperature through time. Only at very high strains, the temperature increased quickly with about 10°C. The authors also illustrated the large increase in engineering strain that could be obtained by executing the tensile test in stirred water at room temperature at a strain rate of 1E-1 s^{-1}. The embrittlement index was corrected with reference tests performed in solution for both materials and is given in Figure 10. It is clear that when the appropriate reference test is used, all conditions led to hydrogen reducing the elongation at fracture.

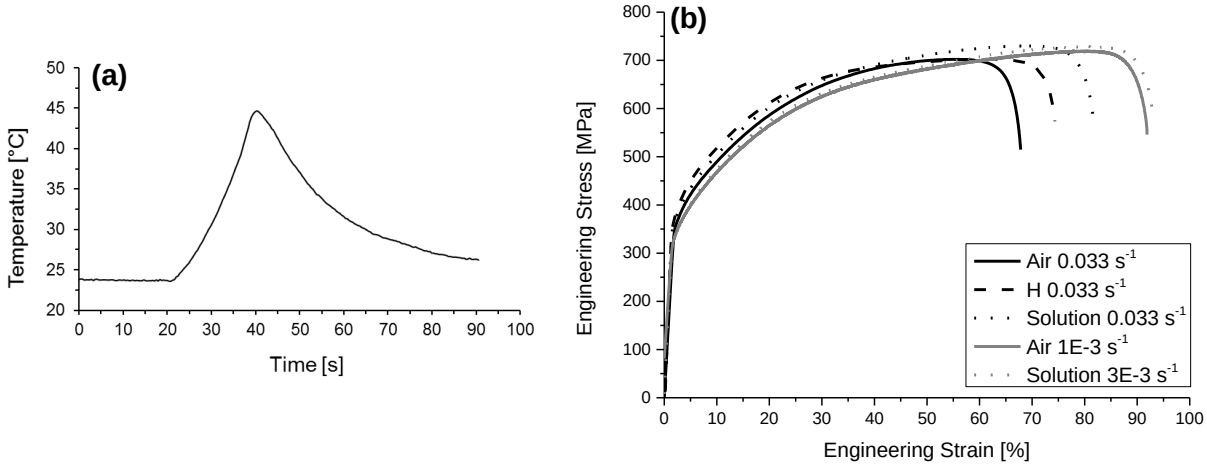

Figure 9: (a) Temperature profile during the air reference test on as-received 304L ASS at 3.3E-2 s^{-1} and (b) Engineering stress-strain curves including reference tests in solution for as-received 304L ASS tested at 3.3E-2 and 1E-3 s^{-1}

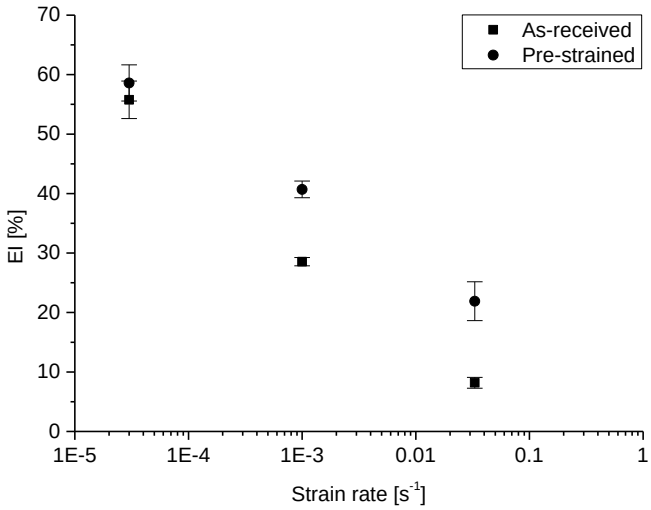

Figure 10: Embrittlement index as a function of strain rate for as-received and pre-strained 304L ASS: solution reference instead of air reference (Figure 8)

3.4 Influence of hydrogen on fracture and deformation

The fractured specimens were subsequently investigated with SEM. The fracture surface of the air tested specimens showed ductile dimples. No clear differences in dimple size and shape were observed for the different strain rates and for whether the 304L ASS was pre-strained or not. Figure 11 (a) shows an example of dimples that were observed on the fracture surface (ND = normal direction) of as-received 304L ASS tested at 1E-3 s^{-1}. The specimens tested with hydrogen showed similar dimples in the center of the fracture surface. The edges were, however, clearly embrittled by hydrogen. For 304 ASS, the type of brittle fracture is stated to depend on the amount of hydrogen in [69]. The fracture surface changes from quasi-cleavage to intergranular fracture. In the present work, quasi-cleavage fracture was observed which is consistent with the used current densities in [69]. An example is shown in Figure 11 (b) for pre-strained 304L ASS tested at a strain rate of 1E-3 s^{-1}. The presence of an embrittled zone near the surface can be interpreted as the location where hydrogen was present in sufficient amounts to alter the fracture behavior. Since the hydrogen concentration was most likely not

enlarged significantly in the center of the specimen during the tensile tests due to diffusion, the fracture surface remained unaffected there."

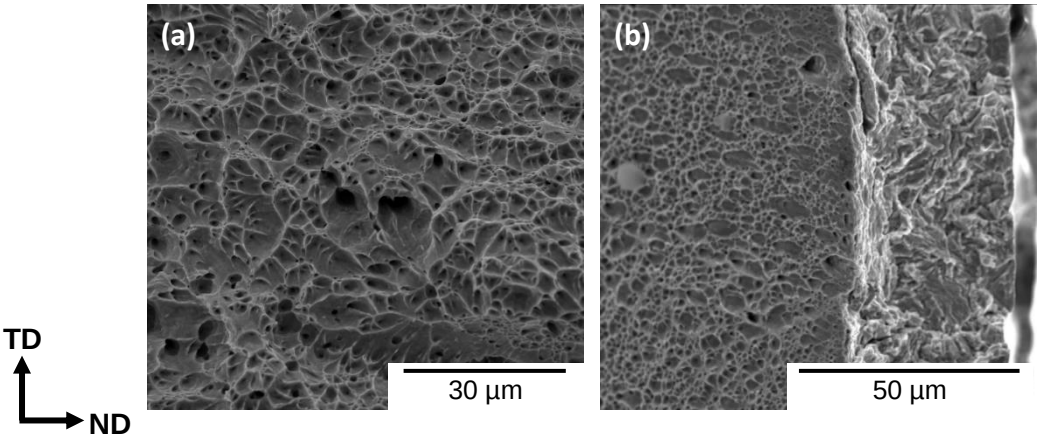

Figure 11: SE images of fracture surface (a) as-received 304L ASS, air, 1E-3 s^{-1}, (b) pre-strained 304L ASS, H, 1E-3 s^{-1}

Depending on the applied strain rate, the size of the embrittled zone was different. The determined sizes are given in Table 4. The size of the brittle zone clearly increased with decreasing strain rate. The hydrogen precharging time was, however, equal for all tests, i.e. the distance hydrogen diffused before the start of the tensile test was equal for all as-received specimens on the one hand and for all pre-strained specimens on the other hand (both approximately 35 µm, cf. Figure 6). However, decreasing the strain rate results in more time for hydrogen to diffuse during the in-situ tensile test and as a result a larger hydrogen embrittled zone. Moreover, as the test is ongoing, more α'-martensite is formed which continuously increases the average hydrogen diffusion coefficient of the material during the course of the experiment. As such, hydrogen can reach deeper into the specimen than expected from the average diffusion coefficient of the materials before the start of the tensile test within the given test durations (see Table 4, approximate test duration). The brittle zones of the pre-strained material were slightly larger than the ones of the as-received 304L ASS. The difference was, however, small which is in agreement with the analysis of the TDS data in Figure 6.

Table 4: Size of the brittle quasi-cleavage zone on hydrogen-tested specimens depending on the strain rate for as received and 30% pre-strained 304L ASS; the approximate tensile test duration with in-situ hydrogen charging was added as well

Strain rate [s^{-1}]	Thickness quasi-cleavage zone [µm]		Approximate test duration (min)	
	As-received	Pre-strained	As-received	Pre-strained
3.3E-2	23-26	24-28	0.4	0.13
1E-3	42-49	40-50	11	3.5
3.3E-5	120-130	128-134	200	75

A further in depth analysis of the variable hydrogen diffusion coefficient as a function of increasing strain was performed to be able to substantiate the observed brittle zones. Olson and Cohen [70] developed a model that describes the evolution of the α'-martensite fraction $f_{\alpha'}$ as a function of the equivalent plastic strain ε:

$$f_{\alpha'} = 1 - \exp\{-\beta[1 - \exp(-\alpha\varepsilon)]^n\}$$

For deformation of 304L ASS at room temperature, the parameters n, β and α were fitted by the authors as 4.5, 3.55 and 0.5, respectively. The fitting ability of this type of equation is fairly good, however, the saturation volume fraction is e.g. not considered. Different modifications were done to the model [71], however, a discussion on the most appropriate model lies out of the scope of this work. The dependency of the hydrogen diffusion coefficient on the α'-martensite fraction in 304L was investigated by several authors as well. In general, the natural logarithm of the diffusion coefficient was found to scale with the natural logarithm of $f_{\alpha'}/(1\text{-}f_{\alpha'})$ [58]. Wang et al. [22] proposed the following expression for the effective hydrogen diffusion coefficient D in 304L ASS valid for $f_{\alpha'} > 0.02$:

$$\ln(D) = 0.811 \ln\left(\frac{f_{\alpha'}}{1 - f_{\alpha'}}\right) - 31.653$$

Combining both equations, yields the effective hydrogen diffusivity as a function of plastic strain ε for 304L ASS. Figure 12 shows the evolution based on the provided literature data. A

value of about 1E-14 m²/s was found for an α'-martensite fraction of 36% which agrees with literature data on duplex stainless steels with 50% ferrite and an effective diffusion coefficient of 2.2E-14 m²/s to 6.4E-14 m²/s [72, 73, 74, 75]. The diffusion depth during the tensile test was subsequently evaluated using both equations. The evolution of the amount of plastic strain was related to the test time through the deformation rate and initial gauge length. Figure 13 shows the result of this analysis. The difference in diffusion depth between the deformation rates clearly reflects the differences that were observed in the size of the brittle zone in Table 4. The used model was found to underestimate the actual size of the brittle zone, especially for the slow deformation rates if one additionally takes into account that a critical hydrogen concentration is needed before the fracture appearance is altered. This difference can be related to the use of the simplified models for both the variation of the fraction of α'-martensite with strain and the hydrogen diffusivity with the α'-martensite fraction, the inaccurate determination of the plastic strain which was thus also not correctly implemented in the model to evaluate the α'-martensite fraction, the presence of stress during the tensile test which influences the hydrogen diffusivity (stress-driven diffusion), the absorption and accumulation of hydrogen directly at the crack tip from the surrounding atmosphere increasing crack growth and the enhanced hydrogen diffusion via dislocation motion during plastic deformation of austenitic steels [76]. Despite the lower test times for the pre-strained 304L ASS, the brittle zone was almost identical in size (cf. Table 4). The effective hydrogen diffusivity most likely evolved faster with plastic strain compared to the as-received 304L ASS which makes sense as the initial α'-martensite fraction as well as many other α'-martensite embryos formed by pre-straining could lead to faster transformation kinetics [77].

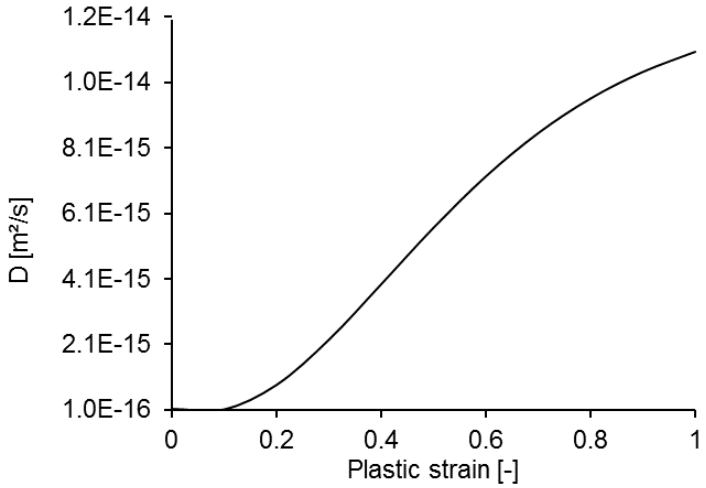

Figure 12: Evolution of the effective hydrogen diffusion coefficient with increasing plastic strain due to an increase of the α'-martensite fraction

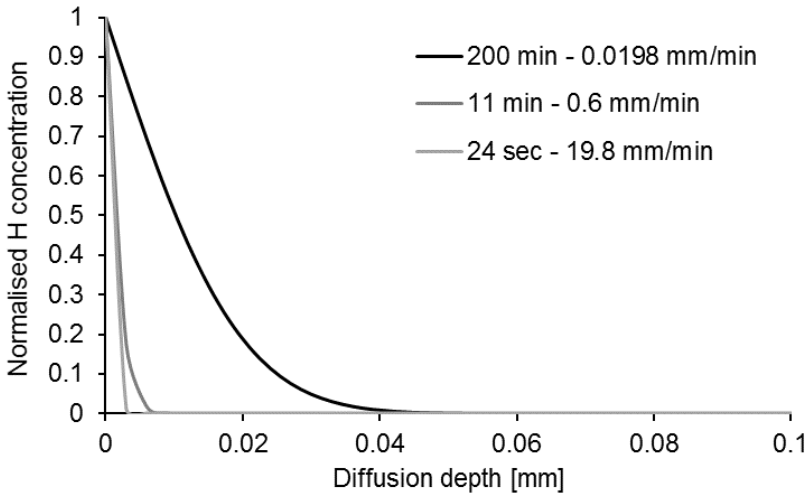

Figure 13: Simplified model to estimate the hydrogen diffusion depth during the tensile tests at different deformation rates for as-received 304L ASS

The normal surface of the fractured specimens showed a lot of deformation when tested in air, as can be seen in the SE image of Figure 14 (a). The hydrogen charged specimens showed deformation as well, however, to a lesser extent. Moreover, they additionally showed many secondary cracks on the normal surface oriented perpendicular to the loading direction. Examples can be found in Figure 14 (b), (c) and (d) for different test conditions (the loading direction was parallel to the rolling direction). Hydrogen-assisted crack (HAC) formation is generally observed when metals are strained under the presence of hydrogen. In austenitic steels, HACs are initiated at extreme slip localizations where the difficulty to cross-slip induces

large stress concentrations [78]. Secondly, HACs initiate at the interface of dynamic α'-martensite islands. Hydrogen diffuses out of the supersaturated transformed α'-martensite to the interface with the austenite matrix where it causes crack initiation [79]. As-received 304L ASS tested at engineering strain rates equal to or higher than 1E-3 s^{-1} showed large cracks over the entire section, cf. Figure 14 (b). The other specimens, i.e. as-received 304L ASS tested at 3.3E-5 s^{-1} and all pre-strained specimens, showed small cracks over the entire section that were not visible at the magnification of Figure 14 (c) and (d). Large, developed cracks were only observed near the fracture surface, i.e. in the zones where the highest strains were reached. The tests that showed the least developed HACs over the entire section reached the lowest elongation at fracture and thus the lowest uniform strains. Only the region that was subjected to necking (and thus high strains) showed large cracks. It should be noted that crack initiation occurred early in the experiment for every material condition and engineering strain rate tested as a result of the high precharged hydrogen concentration over the entire gauge section. Recently, it was reported that subcritical cracking could impact the validity of the used ductility metric (EI) [80]. Materials that showed a superior performance with hydrogen based on this metric showed similar crack initiation times compared to more HE susceptible materials. The interpretation of slow strain rate tensile tests is thus not always unambiguous. For more reliable comparison of the ductility metrics, additional studies are required with an adapted tensile test methodology, i.e. where fracture immediately follows crack initiation.

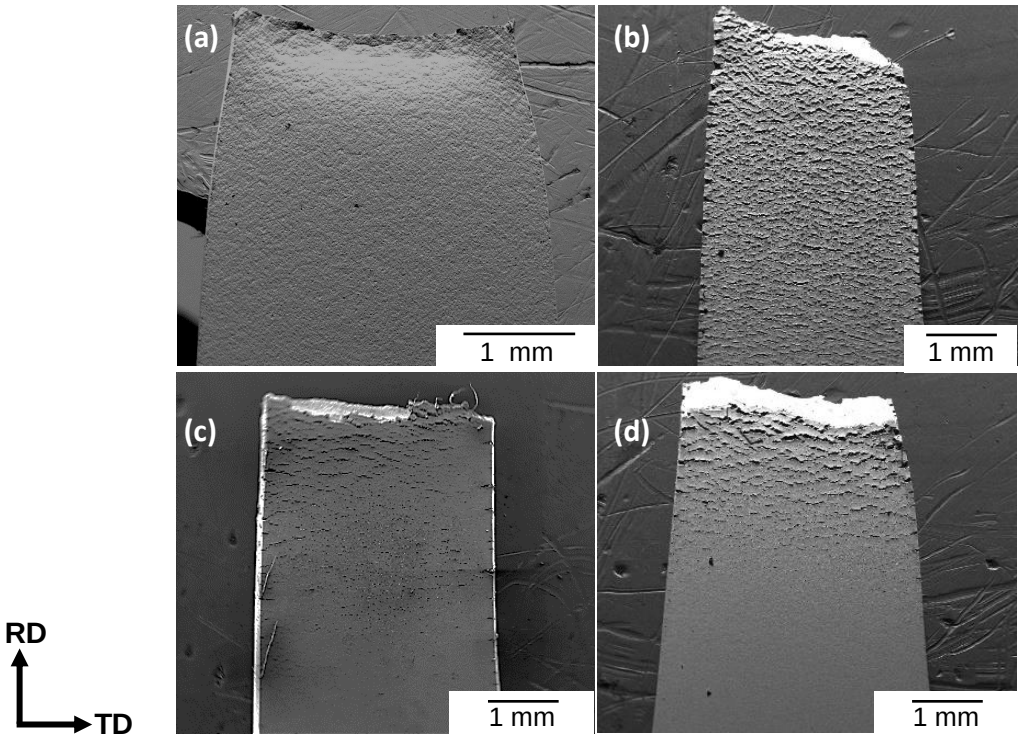

Figure 14: SE images of normal surface of fractured 304L ASS (a) as-received, air, 3.3E-2 s^{-1}, (b) as-received, H, 3.3E-2 s^{-1} (c) as-received, H, 3.3E-5 s^{-1} and (d) pre-strained, H, 1E-3 s^{-1}

EBSD was subsequently used to study the deformed microstructure. Figure 15 shows an EBSD measurement on the normal plane of as-received 304L ASS tested in air at 3.3E-2 s^{-1} and stopped at an intermediate elongation of 30%. The figure clearly indicates that the microstructure was deformed. Several islands of α'-martensite were formed. Deformation at room temperature predominantly initiated the direct γ→α' transformation in 304 ASS [8]. Figure 16 shows an EBSD measurement on the normal plane of as-received 304L ASS that was tested with hydrogen at a strain rate of 3.3E-2 s^{-1}. The test was also interrupted at an elongation of 30%. The black zones are HACs which were extracted from the measurement based on their low image quality. Comparison of Figure 15 and Figure 16 indicates that the deformation process changed significantly under the influence of hydrogen. Increased planar deformation [32] is clearly observable from the image quality map (central image of Figure 16) as many grains showed a lot of straight parallel lines. Since dislocation slip along the {111} planes is heavily promoted, the nucleation and growth of α'-martensite will also be more

planar as the dislocation pile-ups and slip band intersections serving as α'-martensite embryos are formed within these planes and grow by addition of more dislocations to the pile-up or intersecting slip bands [81]. Increased planarity in the α'-martensite fraction was also clearly observed in Figure 16. Moreover, an additional martensitic transformation route was initiated, i.e. γ→ε→α'. This transformation route is typically observed upon transformation of 304L ASS at cryogenic temperatures and is a result of a reduced stacking fault energy (SFE) [82]. This is consistent with previous studies indicating that hydrogen reduced the SFE of FCC steels [83, 84]. As ε-martensite is essentially formed by overlap of intrinsic stacking faults (formed between two partial dislocations) on every second {111} plane, the nucleation and growth of ε-martensite also has a planar appearance [81].

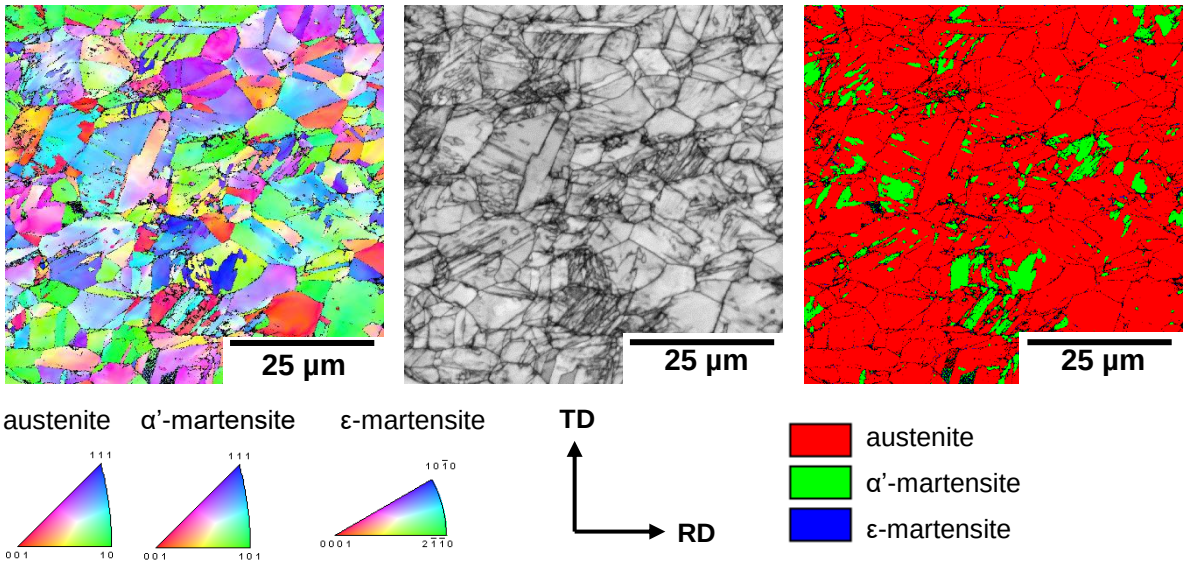

Figure 15: EBSD measurement on ND surface of as-received 304L ASS tested in air at a strain rate of 3.3E-2 s^{-1} stopped at an intermediate elongation of 30%

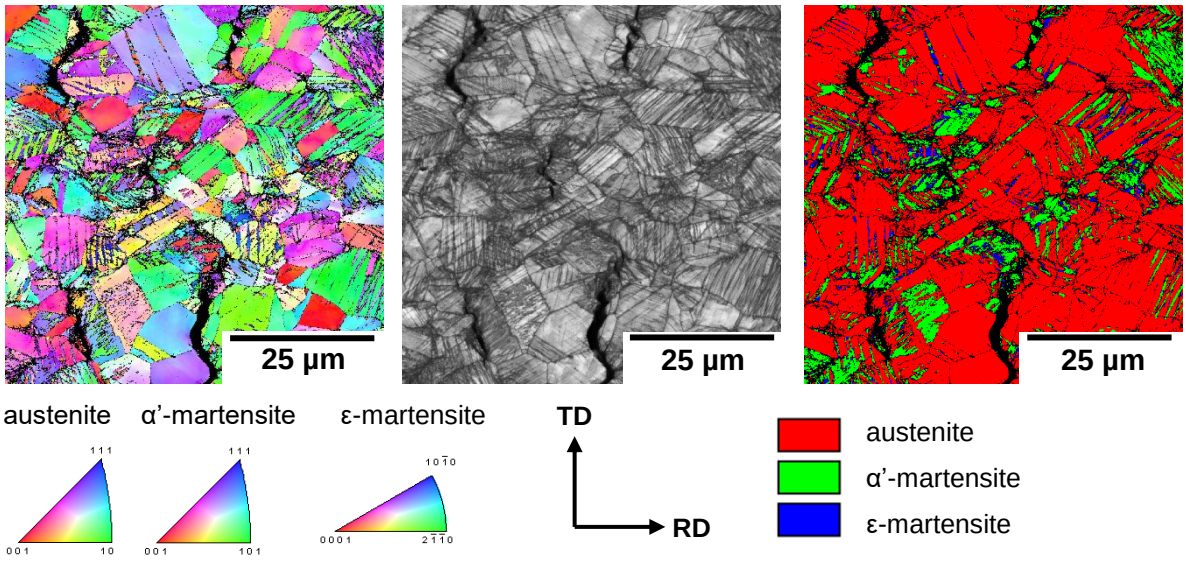

Figure 16: EBSD measurement on ND surface of as-received 304L ASS tested in-situ at a strain rate of 3.3E-2 s^{-1} stopped at an intermediate elongation of 30%, cracks in black

The EBSD measurements indicated that the tests performed with hydrogen showed enhanced martensitic transformations (cf. Figure 15 and Figure 16). A more quantitative study was performed to have an idea on the extent of the martensitic transformations. For this purpose, the martensite fractions were measured by EBSD on the ND plane of specimens tensile tested and stopped at an intermediate elongation of 30%. The reference tests were performed in air for this study. The evolution of the formed martensite fraction as a function of increasing elongation was additionally studied by comparing the 30% elongation data to data of specimens stopped at an intermediate elongation of 60%. Moreover, the center of the TD plane was investigated for the specimens tested at a strain rate of 3.3E-2 s^{-1} as well since hydrogen is expected not to be present there and therefore should not have influenced the martensitic transformations. As the crystallographic orientation with respect to the loading direction should be favorable to have martensitic transformation in individual grains, more than 100 grains were measured within a statistically relevant, constant scan area. The martensite area fractions are reported in Table 5.

Table 5: Martensite area fraction (%) measured with EBSD in different planes (ND and TD plane) at an intermediate elongation of 30% and 60%

		Air		Hydrogen	
		α'-mart [%]	ε-mart [%]	α'-mart [%]	ε-mart [%]
Interrupted at 30%	ND (3.3E-2 s^{-1})	6.4	0.0	16.2	3.2
	ND (1E-3 s^{-1})	5.6	0.0	22.3	4.6
	ND (3.3E-5 s^{-1})	6.5	0.0	20.5	2.5
	TD (center) (3.3E-2 s^{-1})	6.9	0.0	8.2	0.0
Interrupted at 60%	ND (3.3E-2 s^{-1})	17.9	0.0	32.4	4.5
	ND (1E-3 s^{-1})	23.9	0.0	48.3	3.7
	TD (center) (3.3E-2 s^{-1})	20.8	0.0	25.6	0.0

The martensite fractions measured in air are in reasonable agreement with literature data. Similar fractions were reported in the work of Olson and Cohen [70]. Talyan et al. [11] reported α'-martensite fractions slightly lower than 10% for an intermediate strain of 30%. Taking into account the different strain measurements, this is in agreement with the present work as well. From the tensile tests, it was concluded that the air test at 3.3E-2 s^{-1} was prone to an adiabatic heating effect, cf. Figure 9 (a). The martensite fraction on the ND plane at an elongation of 60% for a strain rate of 1E-3 s^{-1} was clearly higher than for the strain rate of 3.3E-2 s^{-1}. The difference was not yet visible at an elongation of 30% in the present work which is most likely due to the martensitic transformations being more active at higher strains and the higher temperature at higher strains. Table 5 indicates a slightly higher martensite fraction in the center of the hydrogen charged specimen (due to limited diffusion, no influence of hydrogen is expected there) compared to the center of the reference test specimen in air at an intermediate elongation of 60% for an engineering strain rate of 3.3E-2 s^{-1}. Talyan et al. [11] also observed a higher martensite fraction when testing was performed in stirred water compared to air. The bulk and surface martensite fractions in air are similar which is in agreement with literature works as well [60].

The martensitic transformation was enhanced at the surface of the hydrogen charged specimens compared to the air reference test (see Table 5, ND) for every tested strain rate and intermediate elongation. The α'-martensite fraction clearly increased in the presence of hydrogen. Moreover, an additional fraction of ε-martensite was detected, as already indicated qualitatively in Figure 16. The ε-martensite fraction on the ND surface of 30% versus 60% elongation with hydrogen remained more or less constant. This might indicate that ε-martensite acted as an intermediate phase for the transformation to α'-martensite. The ε-martensite fractions were calculated by a 0.2 CI threshold because visual inspection confirmed that not all erroneous points were excluded by the 0.1 CI threshold. The hydrogen-enhanced martensitic transformation can be explained within the defactant concept as proposed by Kirchheim [85, 86] stating that adding solute atoms reduces defect formation energies as such increasing defect formation rates. In the present material, these defects include stacking faults, dislocations and interfaces between austenite and martensite. It should also be noted that the slip bands and other defects formed during the charging procedure could have served as nucleation sites for the martensitic transformation. The enhanced martensitic transformation is clearly more restricted for the fast strain rate (3.3E-2 s^{-1}) compared to the other two tested strain rates which show similar martensite fractions. This is believed to be due to the limited test time. Hydrogen needs to be able to interact with dislocations to alter the martensite fractions which is more restricted at high deformation rates.

For the tests at a strain rate of 3.3E-2 s^{-1}, the enhanced martensitic transformation at the surface compared to the reference test in air might also be a result of the restricted adiabatic effect in solution. However, the enhancement of the transformation at all strain rates clearly indicates that hydrogen also contributed since no pronounced adiabatic effect was present for the tests at 1E-3 and 3.3E-5 s^{-1}. Moreover, the present authors demonstrated that

hydrogen-induced martensitic transformations occurred in the austenite fraction of ex-situ tested duplex stainless steel, i.e. no solution effect was present in these tests [87]. Finally, the presence of ε-martensite is a direct consequence of the high hydrogen concentration, since, although the adiabatic effect was restricted, the temperature was not actively decreased into a regime where ε-martensite is favored (cf. air tests). The enhanced ε- and α'-martensitic transformation at lower temperatures is a direct result of the reduced stacking fault energy and austenite stability with decreasing temperature, respectively [25, 88].

Enhanced martensitic transformations should, simultaneously with the increase in elongation, be accompanied with an increase in strength level, as clearly observed when comparing the reference tests at 3.3E-2 s^{-1} in air and in solution. However, the effective strength increase with hydrogen was rather limited. The formation of HACs on the normal surface might have an influence on the UTS. Especially at the faster strain rates (above 1E-3 s^{-1}), large HACs over the entire section reduced the cross-sectional area of the specimen. This reduced cross-section decreases the engineering stress level that could be obtained. The engineering stress of the hydrogen charged steel was e.g. higher at low strains but dropped to a similar level as the reference test in air at high strains for as-received 304L tested at 3.3E-2 s^{-1}. Wang et al. [65] discussed the influence of extensive HAC formation on the true stress for an austenitic twinning-induced plasticity steel. The authors proposed to use the force divided by the ductile fracture area instead of using the total area, however, this still results in a discrepancy with reality. A suitable way to treat cases with extensive crack formation is not yet well established. The volume expansion associated with the martensitic transformation was stated to postpone the nucleation of voids or microcracks and to hinder the propagation of cracks [89]. Xiong et al. [90] showed through finite element modelling that in the absence of hydrogen, the volume expansion positively influenced the crack tip propagation since the compressive stresses

introduced at the crack tip retard plastic strain. With hydrogen, however, since the volume expansion aggravated the size of the stress field at crack tips, crack propagation will probably increase when the α'-martensitic transformation occurs. The intermediate transformation to ε-martensite, however, was found to result in a more compatible strain evolution preventing the nucleation and growth of hydrogen-assisted cracks [91]. Teus et al. [92] also concluded that the ε-martensite transformation retards localized deformation which increased the cracking resistance. Koyama et al. [93] stated that the ε-martensite/austenite interface could arrest microcrack propagation although it also served as a preferential crack initiation site. The beneficial effect of hydrogen-enhanced martensitic transformations might thus be dual: (i) it increases work hardening which postpones necking and (ii) it hinders crack propagation because of the introduction of ε-martensite.

A competition thus exists between HE and hydrogen-enhanced strain-induced martensitic transformations in 304L ASS resulting in the observed final elongation and strength level at fracture. A schematic representation of the balance is shown in Figure 17. The negative contributions prevailed in the present work for every tested condition. The dominating HE mechanism (HEDE, HESIV, HELP) might differ for the tested engineering strain rates. Due to the limited time for diffusion, the ability of hydrogen to assist crack propagation is more limited at high strain rates. It should be noted that the HEDE mechanism does not necessarily need large-scale hydrogen diffusion leading to accumulation of hydrogen at crack tips since the hydrogen concentration in the present work was high from the start and might already have exceeded the critical value for decohesion at low stresses. The abundant presence of HACs on the surface of as-received 304L ASS tested at 3.3E-2 s^{-1} proves this statement (cf. Figure 14). Most likely, the HEDE mechanism dominates at high strain rates and hydrogen concentrations, while the plasticity-mediated mechanisms (HELP, HESIV) increase in

importance at lower strain rates. The size of the enhanced strain-induced martensitic transformation effect depends on the hydrogen concentration whereby a higher hydrogen concentration increases the amount of martensite. Possibilities remain for optimizing the balance between HE and enhanced martensitic transformations in austenitic stainless steels. A steel in which hydrogen enhances martensitic transformations but shows low HE and crack initiation sensitivity, as such sustaining the plastic stress until the plastic instability condition is satisfied, could lead to improved strength/ductility combinations. As the transformations that occurred in the near surface region in the present work are not expected to influence the macroscopic stress/strain behavior largely, moderate hydrogen concentrations should be able to favor martensitic transformations through the entire cross-section in order to have a macroscopic effect. As long as the main martensite fraction upon transformation consists of α'-martensite with a high hydrogen diffusivity, achieving drastic improvement in HE resistance will probably be challenging. Due to the microcrack arrestability, the large strain compatibility with the matrix and the low hydrogen diffusivity of ε-martensite [94], the γ→ε-martensite transformation route should be preferred. The hexagonal close packed (HCP) structure has, however, a lower stress accommodation capacity which means that the ductility of the formed ε-martensite phase is key in maximizing the positive effect [95]. The possible outcome could be similar to the observation by several authors that the presence of hydrogen increased the elongation at fracture in FCC materials by promoting deformation twinning [96, 97, 98]. Both electrochemical and gaseous hydrogen charging were applied in these studies. Deformation twinning is an alternative deformation mechanism and can be treated similarly as ε-martensite with respect to the dislocation processes governing the nucleation and growth. Ogawa et al. [98] state that they were the first to establish prevailing beneficial hydrogen effects in a commercially-available stable austenitic steel. The authors also concluded that the

hydrogen concentration was very important for the final elongation at fracture; more hydrogen (up to 133 wppm) leading to a higher twin fraction and consequently a higher elongation in their work.

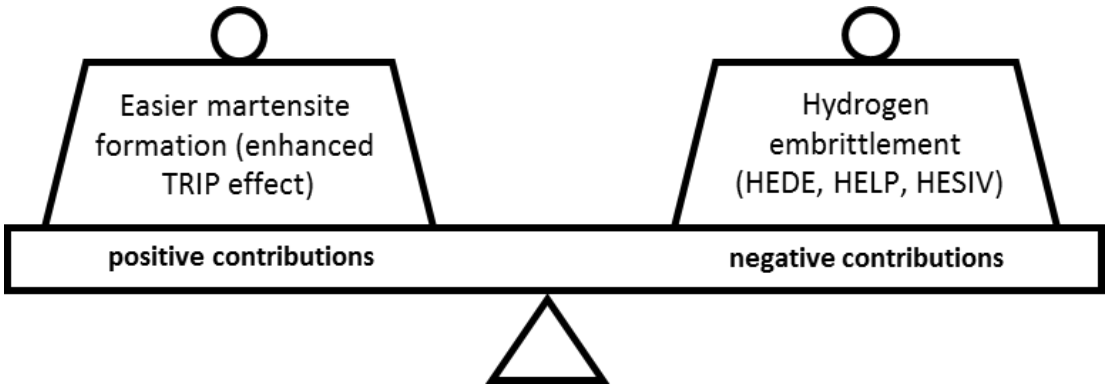

Figure 17: Schematic representation of the balance between the positive and negative contributions of hydrogen on the mechanical properties

4. Conclusion

The HE sensitivity of as-received and 30% pre-strained AISI 304L ASS was evaluated by tensile testing at different constant crosshead displacement rates. The following conclusions were drawn:

- The lower the engineering strain rate, the more the alloy was embrittled as hydrogen was given more time to diffuse and accumulate. As a consequence of the increased diffusion, the size of the embrittled zone on the fracture surface increased with decreasing strain rate as well. Pre-straining increased the HE sensitivity at every strain rate due to the presence of stress concentrations and possibly a faster increase of the α'-martensite fraction with strain.
- Hydrogen-assisted cracking was observed on the normal surface. The cracks increased in size depending on the amount of strain that could be reached at fracture.
- At an engineering strain rate of 3.3E-2 s^{-1}, an increase in elongation at fracture was observed for as-received 304L ASS tested in-situ with hydrogen compared to the

reference air test. Compared to the reference test in solution, embrittlement was observed. This was a result of the restriction of the adiabatic heating effect in solution.

- Enhanced martensitic transformations were observed at the surface in the presence of hydrogen. Apart from an increased α'-martensite fraction, ε-martensite was additionally formed. A reduction in stacking fault energy and austenite stability were held responsible.
- HE of unstable austenitic stainless steels should be evaluated at comparable conditions, i.e. both in air or both in solution, for fast strain rates (>1E-3 s^{-1}).

5. Acknowledgement

The authors wish to thank Amber Coone for her experimental work performed in the framework of this research. Furthermore, the authors acknowledge support from FWO (SB PhD fellow grant 1S16620N and senior postdoctoral fellow grant 12ZO420N) and from the special research fund (BOF) of Ghent University (grant BOF15/BAS/062 and BOF01P03516). The authors would also like to acknowledge Aperam for the supplied material.

6. References

[1] „AISI 304 (S30400) Stainless Steel," MakeItFrom, 18 October 2018. [Online]. Available: https://www.makeitfrom.com/material-properties/AISI-304-S30400-Stainless-Steel. [Geopend 7 January 2020].

[2] P. Decléty, „Metals used in the food industry," in *Encyclopedia of food sciences and nutrition (second edition)*, Vernouillet, Academic press, 2003, pp. 3869-3876.

[3] J. Talonen, P. Nenonen, G. Pape en H. Hänninen, „Effect of strain rate on the strain-induced gamma -> alpha prime martensite transformation and mechanical properties of austenitic stainless steels," *Metallurgical and materials transactions,* vol. 36, pp. 421-432, 2005.

[4] F. Fischer, E. Oberaigner, K. Tanaka en F. Nishimura, „Transformation induced plasticity revised an updated formulation," *International journal of solids and structures,* vol. 35, nr. 18, pp. 2209-2227, 1998.

[5] Y. Li, F. Bu, W. Kan en H. Pan, „Deformation-induced martensitic transformation behavior in cold-rolled AISI 304 stainless steels," *Materials and manufacturing processes,* vol. 28, nr. 3, 2012.

[6] A. Das , S. Sivaprasad, M. Ghosh, P. Chakraborti en S. Tarafder, „Morphologies and characteristics of deformation induced martensite during tensile deformation of 304LN stainless steel," *Materials science and engineering A,* vol. 486, pp. 283-286, 2008.

[7] D. Kaoumi en J. Liu, „Deformation induced martensitic transformation in 304 austenitic stainless steel: In-situ vs. ex-situ transmission electron microscopy characterization," *Mateials science and engineering A,* vol. 715, pp. 73-82, 2018.

[8] J. Rodriguez-Martinez, R. Pesci en A. Rusinek, „Experimental study on the martensitic transformation in AISI 304 steel sheets subjected to tension under wide ranges of strain rate at room temperature," *Materials science and engineering A,* vol. 528, pp. 5974-5982, 2011.

[9] G. Olson en M. Cohen, „A mechanism for the strain-induced nucleation of martensitic transformations," *Journal of the less-common metals,* vol. 28, pp. 107-118, 1972.

[10] J. Buckley en D. Hardie, „The effect of pre-straining and delta-ferrite on the embrittlement of 304L stainless steel by hydrogen," *Corrosion science,* vol. 34, nr. 1, pp. 93-107, 1993.

[11] V. Talyan, R. Wagoner en J. Lee, „Formability of stainless steel," *Metallurgical and materials transactions A,* vol. 29, pp. 2161-2172, 1998.

[12] S. Hecker, M. Stout, K. Staudhammer en J. Smith, „Effects of strain state and strain rate on deformation-induced transformation in 304 stainless steel: part I. Magnetic measurements and mechanical behaviour," *Metallurgical transactions A,* vol. 13, pp. 619-626, 1982.

[13] C. San Marchi, „Technical reference on hydrogen compatibility of materials: Austenitic stainless steels type 304 and 304L," Sandia national laboratories, Livermore, 2005.

[14] H. Birnbaum en P. Sofronis, „Hydrogen-enhanced localized plasticity - a mechanism for hydrogen-related fracture," *Materials science and engineering A,* vol. 176, pp. 191-202, 1994.

[15] R. Oriani, „A mechanistic theory of hydrogen embrittlement of steels," *Berichte der Bundengesellschaft für physikalische chemie,* vol. 76, nr. 8, pp. 848-857, 2010.

[16] M. Hatano, M. Fujinami, K. Arai, H. Fujii en M. Nagumo, „Hydrogen embrittlement of austenitic stainless steels revealed by deformation microstructures and strain-induced creation of vacancies," *Acta materialia,* vol. 67, pp. 342-353, 2014.

[17] A. Brass en J. Chene, „Influence of deformation on the hydrogen behavior in iron and nickel base alloys: a review of experimental data," *Materials science and engineering A,* vol. 242, pp. 210-221, 1998.

[18] C. Pan, W. Chu, Z. Li, D. Liang, Y. Su, K. Gao en L. Qiao, „Hydrogen embrittlement induced by atomic hydrogen and hydrogen-induced martensites in type 304L stainless steel," *Materials science and engineering A,* vol. 351, pp. 293-298, 2003.

[19] T. Michler, C. San Marchi, J. Naumann, S. Weber en M. Martin, „Hydrogen environment embrittlement of stable austenitic steels," *International journal of hydrogen energy,* vol. 37, nr. 21, pp. 16231-16246, 2012.

[20] C. Briant, „Hydrogen assisted cracking of type 304 stainless steel," *Metallurgical transactions A,* vol. 10, pp. 181-189, 1979.

[21] G. Han, J. He, S. Fukuyama en K. Yokogawa, „Effect of strain-induced martensite on hydrogen environment embrittlement of sensitized austenitic stainless steels at low temperatures," *Acta materialia,* vol. 46, nr. 13, pp. 4559-4570, 1998.

[22] Y. Wang, X. Wang, J. Gong, L. Shen en W. Dong, „Hydrogen embrittlement of cathodically hydrogen-precharged 304L austenitic stainless steel: effect of plastic pre-strain," *International journal of hydrogen energy,* vol. 39, pp. 13909-13918, 2014.

[23] Y. Wang, X. Wu en W. Wu, „Effect of alpha prime martensite content induced by tensile plastic prestrain on hydrogen transport and hydrogen embrittlement of 304L austenitic stainless steel," *Metals,* vol. 8, nr. 9, pp. 660-682, 2018.

[24] C. Lai, L. Tsay en C. Chen, „Effect of microstructure on hydrogen embrittlement of various stainless steels," *Materials science and engineering A,* vol. 584, pp. 14-20, 2013.

[25] D. Eliezer, D. Chakrapani, C. Altstetter en E. Pugh, „The influence of austenite stability on the hydrogen embrittlement and stress-corrosion cracking of stainless steel," *Metallurgical transactions A,* vol. 10, pp. 935-941, 1979.

[26] T.-P. Perng en C. Altstetter, „Cracking kinetics of two-phase stainless steel alloys in hydrogen gas," *Metallurgical transactions A,* vol. 19, nr. 1, pp. 145-152, 1988.

[27] M. Martin, S. Weber, C. Izawa, S. Wagner, A. Pundt en W. Theisen, „Influence of machining-induced martensite on hydrogen-assisted fracture of AISI type 304 austenitic stainless steel," *International journal of hydrogen energy,* vol. 36, pp. 11195-11206, 2011.

[28] X. Sun, L. Xu en Y. Li, „Hydrogen permeation behaviour in austenitic stainless steels," *Materials science and engineering A,* vol. 14, pp. 179-187, 1989.

[29] L. Zhang, Z. Li, J. Zheng, Y. Zhao, P. Xu, C. Zhou en X. Li, „Effect of strain-induced martensite on hydrogen embrittlement of austenitic stainless steels investigated by combined tension and hydrogen release methods," *International journal of hydrogen energy,* vol. 38, pp. 8208-8214, 2013.

[30] C. Zhou, Y. Song, Q. Shi, S. Hu, J. Zheng, P. Xu en L. Zhang, „Effect of pre-strain on hydrogen embrittlement of metastable austenitic stainless steel under different hydrogen conditions," *International journal of hydrogen energy,* vol. 44, pp. 26036-26048, 2019.

[31] P. Ferreira, I. Robertson en H. Birnbaum, „Hydrogen effects on the interaction between dislocations," *Acta Materialia,* vol. 46, pp. 1749-1757, 1998.

[32] K. Nibur, D. Bahr en B. Somerday, „Hydrogen effects on dislocation activity in austenitis stainless steel," *Acta materialia,* vol. 54, pp. 2677-2684, 2006.

[33] P. Ferreira, I. Robertson en H. Birnbaum, „Hydrogen effects on the character of dislocations in high-purity aluminium," *Acta materialia,* vol. 47, nr. 10, pp. 2991-2998, 1999.

[34] X. Lu, Y. Ma, M. Zamanzade, Y. Deng, D. Wang, W. Bleck, W. Song en A. Barnoush, „Insight into hydrogen effect on a duplex medium-Mn steel revealed by in-situ nanoindentation test," *International journal of hydrogen energy,* vol. 44, 2019.

[35] S. Bak, M. Abro en D. Lee, „Effect of hydrogen and strain-induced martensite on mechanical properties of AISI 304 stainless steel," *Metals,* vol. 6, p. 169, 2016.

[36] Y. Mine, Z. Horita en Y. Murakami, „Effect of hydrogen on martensite formation in austenitic stainless steels in high-pressure torsion," *Acta materialia,* vol. 57, nr. 10, pp. 2993-3002, 2009.

[37] Y. Kim, S. Bak en S. Kim, „Effect of strain-induced martensite on tensile properties and hydrogen embrittlement of 304 stainless steel," *Metallurgical and materials transactions A,* vol. 47, pp. 222-230, 2016.

[38] P. Rozenak, I. Robertson en H. Birnbaum, „HVEM studies of the effects of hydrogen on the deformation and fracture of AISI type 316 austenitic stainless steel," *Acta metallurgica and materialia,* vol. 38, nr. 1, pp. 2031-2040, 1990.

[39] E. Astafurova, S. Astafurov, G. Maier, V. Moskvina, E. Melnikov en A. Fortuna, „Hydrogen embrittlement of ultrafine-grained austenitic stainless steels," *Rev. Adv. Mater. Sci.,* vol. 54, pp. 25-45, 2018.

[40] K. Verbeken, N. Van Caenegem en D. Raabe, „Identification of epsilon martensite in a Fe-based shape memory alloy by means of EBSD," *Micron,* vol. 40, nr. 1, pp. 151-156, 2009.

[41] K. Verbeken, N. Van Caenegem en M. Verhaege, „Quantification of the amount of epsilon martensite in a Fe-Mn-Si-Cr-Ni shape memory alloy by means of electron backscatter diffraction," *Materials science and engineering A - structural materials properties, microstructure and processing,* vol. 481, pp. 471-475, 2008.

[42] L. Claeys, T. Depover, I. De Graeve en K. Verbeken, „Electrochemical hydrogen charging of duplex stainless steel," *Corrosion,* vol. 75, nr. 8, pp. 880-887, 2019.

[43] M. Enomoto, L. Cheng, H. Mizuno, Y. Watanabe, T. Omura, J. Sakai, K. Yokoyama, H. Suzuki en R. Okuma, „Hydrogen absorption into austenitic stainless steels under high-pressure gaseous hydrogen and cathodic charge in aqueous solution," *Metallurgical and materials transactions E,* vol. 1, pp. 331-340, 2014.

[44] L. Claeys, V. Cnockaert, T. Depover, I. De Graeve en K. Verbeken, „Critical assesment of the evaluation of thermal desorption spectroscopy data for duplex stainless steels: a combined experimental and numerical approach," *Acta Materialia,* vol. 186, pp. 190-198, 2020.

[45] D. Field, „Recent advances in the application of orientation imaging," *Ultramicroscopy,* vol. 67, pp. 1-9, 1997.

[46] Q. Yang en J. Luo, „Martensite transformation and surface cracking of hydrogen charged and outgassed type 304 stainless steel," *Materials science and engineering A,* vol. 288, pp. 75-83, 2000.

[47] M. Holzworth en M. Louthan, „Hydrogen-induced phase transformations in type 304L stainless steels," *Corrosion,* vol. 24, pp. 110-124, 1968.

[48] N. Narita, C. Altstetter en H. Birnbaum, „Hydrogen-related phase transformations in austenitic stainless steels," *Metallurgical transactions A,* vol. 13, pp. 1355-1365, 1982.

[49] Q. Yang, L. Qiao, S. Chiovelli en J. Luo, „Critical hydrogen charging conditions for martensite transformation and surface cracking in type 304 stainless steel," *Scripta materialia,* vol. 40, nr. 11, pp. 1209-1214, 1999.

[50] A. Barnoush, M. Zamanzade en H. Vehoff, „Direct observation of hydrogen-enhanced plasticity in super duplex stainless steel by means of in situ electrochemical methods," *Scripta materialia,* vol. 62, pp. 242-245, 2010.

[51] T. Depover, E. Wallaert en K. Verbeken, „Fractographic analysis of the role of hydrogen diffusion on the hydrogen embrittlement susceptibility of DP steel," *Materials science and engineering A,* vol. 649, pp. 201-208, 2016.

[52] G. Caskey en R. Sisson, „Hydrogen solubility in austenitic stainless steels," *Scripta metallurgica,* vol. 15, pp. 1187-1190, 1981.

[53] C. San Marchi, B. Somerday en S. Robinson, „Permeability, solubility and diffussivity of hydrogen isotopes in stainless steels at high gas pressures," *International journal of hydrogen energy,* vol. 32, pp. 100-116, 2007.

[54] R. Kirchheim, „Bulk diffusion-controlled thermal desorption spectroscopy with examples for hydrogen in iron," *Metallurgical and materials transactions A,* vol. 47, pp. 672-696, 2016.

[55] Y. Mine, Z. Horita en Y. Murakami, „Effect of hydrogen on martensite formation in austenitic stainless steels in high-pressure torsion," *Acta Materialia,* vol. 57, pp. 2993-3002, 2009.

[56] V. Polyanskiy, A. Belyaev, E. Alekseeva, A. Polyanskiy, D. Tretyakov en Y. Yakovlev, „Phenomenon of skin effect in metals due to hydrogen absorption," *Continuum mechanics and thermodynamics,* vol. 31, pp. 1961-1975, 2019.

[57] S. Xiukui, X. Jian en L. Yiyi, „Hydrogen permeation behaviour in austenitic stainless steels," *Materials science and engineering A,* vol. 114, pp. 179-187, 1989.

[58] T.-P. Perng en C. Altstetter, „Effects of deformation on hydrogen permeation in austenitic stainless steels," *Acta metallurgica,* vol. 34, nr. 9, pp. 1771-1781, 1986.

[59] T. Omura, J. Nakamura, H. Hirata, K. Jotoku, M. Ueyama, T. Osuki en M. Terunuma, „Effect of surface hydrogen concentration on hydrogen embrittlement properties of stainless steels and Ni based alloys," *ISIJ International,* vol. 56, nr. 3, pp. 405-412, 2016.

[60] J. Lichtenfeld, M. Mataya en C. Van Tyne, „Effect of strain rate on stress-strain behavior of alloy 309 and 304L austenitic stainless steel," *Metallurgical and materials transactions A,* vol. 37, pp. 147-161, 2006.

[61] A. Das, S. Sivaprasad, P. Chakraborti en S. Tarafder, „Correspondence of fracture surface features with mechanical properties in 304LN stainless steel," *Materials science and engineering A,* vol. 496, pp. 98-105, 2008.

[62] X. Li, J. Chen, L. Ye, W. Ding en P. Song, „Influence of strain rate on tensile characteristics of SUS304 metastable austenitic stainless steel," *Acta Metall. Sin. (Engl. Lett.),* vol. 26, nr. 6, pp. 657-662, 2013.

[63] I. Tamura, „Deformation-induced martensitic transformation and transformation-induced plasticity in steels," *Metal Science,* vol. 16, nr. 5, pp. 245-253, 1982.

[64] Z.-Y. Xue, S. Zhou en X.-C. Wei, „Influence of pre-transformed martensite on work hardening behavior of SUS 304 metastable austenitic stainless steel," *Journal of iron and steel research international,* vol. 17, nr. 3, pp. 51-55, 2010.

[65] D. Wang, X. Lu, X. Guo en R. Johnsen, „Effect of hydrogen on the embrittlement susceptibility of Fe-22Mn-0.6C TWIP steel revealed by in-situ tensite tests," *Materials science and engineering A,* vol. 802, p. 140638, 2021.

[66] Y. Momotani, A. Shibata, D. Terada en N. Tsuji, „Effect of strain rate on hydrogen embrittlement in low-carbon martensitic steel," *International journal of hydrogen energy,* vol. 42, nr. 5, pp. 3371-3379, 2017.

[67] T. Depover, F. Vercruysse, A. Elmahdy, P. Verleysen en K. Verbeken, „Interpretation of the hydrogen effect on the static and dynamic tensile behaviour of dual phase steel," *Proceedings Steel y hydrogen,* vol. D03, 2018.

[68] Y. Wang, X. Li, D. Dou, L. Shen en J. Gong, „FE analysis of hydrogen diffusion around a crack tip in an austenitic stainless steel," *International journal of hydrogen energy,* vol. 41, pp. 6053-6063, 2016.

[69] X. Li, B. Gong, C. Deng en Y. Li, „Failure mechanism transition of hydrogen embrittlement in AISI 304 K-TIG weld metal under tensile loading," *Corrosion Science,* vol. 130, pp. 241-251, 2018.

[70] G. Olson en M. Cohen, „Kinetics of strain-induced martensitic nucleation," *Metallurgical transactions A,* vol. 6, pp. 791-795, 1975.

[71] M. Sohrabi, M. Naghizadeh en H. Mirzadeh, „Deformation-induced martensite in austenitic stainless steels: a review," *Archives of civil and mechanical engineering ,* vol. 20, nr. 4, p. 124, 2020.

[72] W. Luu, P. Liu en P. Wu, „Hydrogen transport and degradation of a commercial duplex stainless steel," *Corrosion science,* vol. 44, pp. 1783-1791, 2002.

[73] S. Chen, T. Wu en J. Wu, „Effects of deformation on hydrogen degradation in a duplex stainless steel," *Journal of materials science,* vol. 39, pp. 67-71, 2004.

[74] S.-L. Chou en W.-T. Tsai, „Effect of grain size on the hydrogen-assisted cracking in duplex stainless steels," *Materials science and engineering A,* vol. 270, pp. 219-224, 1999.

[75] J. Zelinski en C. San Marchi, „Technical reference on hydrogen compatibility of materials: high alloy ferritic steels: duplex stainless steels," Sandia national laboratories, Livermore, 2008.

[76] S. Pu en S. Ooi, „Hydrogen transport by dislocation movement in austenitic steel," *Materials science and engineering A,* vol. 761, p. 138059, 2019.

[77] K. Spencer, J. Embury, K. Conlon, M. Véron en Y. Bréchet, „Strengthening via the formation of strain-induced martensite in stainless steels," *Materials science and engineering A,* Vols. %1 van %2387-389, pp. 873-881, 2004.

[78] D. Ulmer en C. Altstetter, „Hydrogen-induced strain localization and failure of austenitic stainless steels at high hydrogen concentrations," *Acta metall. mater.,* vol. 39, nr. 6, pp. 1237-1248, 1991.

[79] L. Zhang, S. Fukuyama, T. Iilima en K. Yokogawa, „Characterization of hydrogen-induced crack initiation in metastable austenitic stainless steels during deformation," *Journal of applied physics,* vol. 108, pp. 063526-1-4, 2010.

[80] E. Martinez-paneda, Z. Harris, S. Fuentes-Alonso, J. Scully en J. Burns, „On the suitability of slow strain rate tensile testing for assessing hydrogen embrittlement susceptibility," *Corrosion Science,* vol. 163, p. 108291, 2020.

[81] J. Brooks, M. Loretto en R. Smallman, „Direct observation of martensite nuclei in stainless steel," *Acta metallurgica,* vol. 27, pp. 1839-1847, 1979.

[82] A. Weis, H. Gutte en J. Mola, „Contributions of epsilon and alfa prime TRIP effects to the strength and ductility of AISI 304 (X5CrNi18-10) austenitic stainless steel," *metallurgical and materials transactions A,* vol. 47, pp. 112-122, 2016.

[83] A. Pontini en J. Hermida, „X-ray diffraction measurement of the stacking fault energy reduction induced by hydrogen in an AISI 304 steel," *Scripta materialia,* vol. 37, nr. 11, pp. 1831-1837, 1997.

[84] P. Ferreira, I. Robertson en H. Birnbaum, „Influence of hydrogen on the stacking fault energy of an austenitic stainless steel," *Materials Science Forum,* Vols. %1 van %2207-209 (PART I), pp. 93-96, 1996.

[85] R. Kirchheim, „Reducing grain boundary, dislocation line and vacancy formation energies by solute segregation II. Experimental evidence and consequences," *Acta materialia,* vol. 55, pp. 5139-5148, 2007.

[86] R. Kirchheim, „Revisiting hydrogen embrittlement models and hydrogen-induced homogeneous nucleation of dislocations," *Scripta materialia,* vol. 62, pp. 67-70, 2010.

[87] L. Claeys, T. Depover, I. De Graeve en K. Verbeken, „First observation by EBSD of martensitic transformations due to hydrogen presence during straining of duplex stainless steel," *Materials characterization,* vol. 156, 2019.

[88] L. Rémy, A. Pineau en B. Thomas, „Temperature dependence of stacking fault energy in close-packed metals and alloys," *Materials science and engineering ,* vol. 36, nr. 1, pp. 47-63, 1978.

[89] P. Jaques, Q. Furnémont, T. Pardoen en F. Delannay, „On the role of martensitic transformation on damage and cracking resistance in TRIP-assisted multiphase steels," *Acta Materialia,* vol. 49, pp. 139-152, 2001.

[90] Z. Xiong, W. Zheng, Y. Liu, Y. Kuang en J. Yang, „Hydrogen diffusion mechanism around a crack tip in Type 304L austenite strainless steel considering the influence of volume expansion of strain-induced martensite transformation," *metals,* vol. 9, pp. 977-986, 2019.

[91] Y. Li, W. Li, J. Hu, H. Song en X. Jin, „Compatible strain evolution in two phases due to epsilon martensite transformation in duplex TRIP-assisted stainless steels with high hydrogen embrittlement resistance," *International journal of plasticity,* vol. 88, pp. 53-69, 2017.

[92] S. Teus, V. Shyvanyuk en V. Gavriljuk, „Hydrogen-induced gamma to epsilon transformation and the role of epsilon martensite in hydrogen embrittlement of austenitic steels," *Materials science and engineering A,* vol. 497, pp. 290-294, 2008.

[93] M. Koyama, S. Okazaki, T. Sawaguchi en K. Tsuzaki, „Hydrogen embrittlement susceptibility of Fe-Mn binary alloys with high Mn content: effects of stable and metastable epsilon-martensite and Mn concentration," *Metallurgical and materials transactions A,* vol. 47, pp. 2656-2673, 2016.

[94] K. Hirata, S. Iikubo, M. Koyama, K. Tsuzaki en H. Ohtani, „First-principles study on hydrogen diffusivity in BCC, FCC and HCP iron," *Metallurgical and materials transactions A,* vol. 49, nr. 10, pp. 5015-5022, 2018.

[95] M. Koyama, T. Eguchi, K. Ichii, C. Tasan en K. Tsuzaki, „A new design concept for prevention of hydrogen-induced mechanical degradation: viewpoints of metastability and high entropy," *Procedia structural integrity,* vol. 13, pp. 292-297, 2018.

[96] H. Luo, Z. Li en D. Raabe, „Hydrogen enhances strength and ductility of an equiatomic high-entropy alloy,” *Nature scientific reports,* vol. 7, p. 7, 2017.

[97] K. Yamada, M. Koyama, T. Kaneko en K. Tsuzaki, „Positive and negative effects of hydrogen on tensile behaviour in polycrystalline Fe-30Mn-(6-x)Si-xAl austenitic alloys,” *Scripta materialia,* vol. 105, pp. 54-57, 2016.

[98] Y. Ogawa, H. Hosoi, K. Tsuzaki, T. Redarce, O. Takakuwa en H. Matsunaga, „Hydrogen, as an alloying element, enables a greater strength-ductility balance in an Fe-Cr-Ni-based, stable austenitic stainless steel,” *acta materialia,* 2020.